Tribology International, Volume 195, July 2024, Article number 109647
DOI:10.1016/j.triboint.2024.109647

Randomised nano-/micro- impact testing – a novel experimental test method to simulate erosive damage caused by solid particle impacts

Ben D. Beake[1,*], Stephen R. Goodes[1], Hannah Zhang[2], Luis Isern[3], Christine Chalk[3], John R. Nicholls[3] and Mark G. Gee[2].

1 Micro Materials Ltd., Willow House, Yale Business Village, Ellice Way, Wrexham, LL13 7YL, UK

2 National Physical Laboratory, Hampton Road, Teddington, Middlesex, TW11 0LW, UK

3 Surface Engineering and Precision Centre (SEPC), School of Aerospace, Transport and Manufacturing, Building 57, Cranfield University, Cranfield, Bedfordshire, MK43 0AL, UK

*Corresponding author: Tel: +44 1978 261615 (B.D. Beake); e-mail: ben.beake@micromaterials.co.uk (B.D. Beake)

Abstract

A novel randomised nano-/micro-scale impact test method has been developed to experimentally simulate particulate erosion where statistically distributed impacts with defined energy occur sequentially within the test area. Tests have been performed on two brittle glasses (fused silica and BK7) to easily highlight the interaction between impacts, as well as on two ceramic thermal barrier coating systems (TBCs, yttria stabilised zirconia, 7YSZ, and gadolinium zirconate, GZO) that experience erosion in service. Differences in erosion resistance were reproduced in the randomised impact tests, with GZO less impact resistant than 7YSZ, and BK7 significantly worse than fused silica. The impact data show that erosion resistance is influenced by different factors for the glasses (crack morphology, longer-length interaction of radial-lateral cracks in BK7 vs cone-cracking in fused silica) and TBCs (fracture toughness).

Keywords: Erosion, thermal barrier coating, impact, wear.

1. Introduction

Improving our understanding of how solid particle erosion proceeds step-by-step and how damage from previous contacts influences subsequent cracking and material removal is important in designing damage-tolerant, impact-resistant surfaces. Solid particle erosion occurs by damage accumulation through the impact of many particles on a surface [1-3]. Consideration of the mechanics of deformation by single particle impacts has improved our understanding of erosion processes, particularly for thermal barrier coatings (TBCs) in jet engines [4-11]. Hutchings proposed equations based on combinations of hardness, elastic modulus and toughness which could be used to generate deformation maps with zones of plastic deformation, plastic flow, Hertzian fracture and lateral fracture being dependent on the size and velocity of the impact particles [1]. In some cases, it has been possible to reduce erosion loading sufficiently that discrete damage caused by single particle impact can be observed. However, such studies do not directly address how solid particle erosion proceeds step-by-step and how damage generated by previous contacts influences subsequent cracking and material removal.

There is a pressing need for rapid laboratory-based testing to streamline the development of advanced impact-resistant and damage-tolerant coating systems, such as TBCs in jet engines. Developing advanced coatings for reliable use in these harsh environments is challenging as they must be multifunctional, displaying a range of desirable properties (e.g. low thermal conductivity, high erosion resistance…) that may be antagonistic [11]. Additionally, TBCs are required to show chemical resilience to ingestion of airborne dusts which include runway dusts and volcanic ash and mainly comprise calcia-magnesia-alumina-silicates (CMAS). A particular

problem is that the erosion resistance of TBCs is not particularly high, typically 2-3 times lower than the superalloy to which it is applied [12]. This is compound by the fact that novel coating compositions with the required low thermal conductivity and high resistance to CMAS attack are intrinsically less resistant to erosion than zirconia-based TBCs, so developing strategies to maintain or improve their resistance to high temperature impact and erosion is needed to enable the engines to run hotter. Higher engine operating temperatures will increase the efficiency of gas turbines, saving fuel and reducing CO_2 emissions [13]. Nano- and micro-mechanical test methods have the potential to dramatically speed up and lower the cost of this coating development by enabling many different potential coating compositions to be tested rapidly, with only tiny volumes of material required.

The repetitive nano-impact test has been used to study impact resistance at high strain rate and small scale. The tests are performed with a nanomechanical test platform (NanoTest Vantage) at strain rates approaching 10^5 s^{-1}, several orders of magnitude higher than in quasi-static indentation [14]. Although single indentations with known force and probe geometry have been used to provide some understanding of the role of mechanical properties on erosion [3,15], the accumulation of damage from multiple impacts involves the interaction of crack systems and residual stress fields created by previous contacts which the single indentations do not provide. Cyclic, or repetitive, impact tests can reveal fatigue deformation mechanisms that are not present in single-cycle tests [16,17] and have been employed as model tests for assessing coating durability [18,19]. In this test, the repetitive impacts occur at the same position on the surface and the probe depth recorded for each impact. This has been shown to be a highly efficient method for rapidly generating cracking and failure in brittle and semi-brittle materials such as hard and tough PVD ceramic coatings and bulk ceramics and to study the influence of microstructure on their damage tolerance under varying impact energy and/or test probe geometry [20-22]. Several studies have reported a direct correlation between coating behaviour

in the nano-impact test and their performance in high-speed machining [23-26] and to their erosion resistance [27-29]. Investigations into hard ceramic nitride coatings on cemented carbide tool inserts have noted strong correlation between fracture resistance in the nano-impact test and reduced wear of the coated tools in high-speed machining [23-26]. Chen and co-workers reported that the influence of thermal ageing on the resistance to solid particle erosion of columnar EB-PVD thermal barrier coatings was reproduced in nano-impact [27]. McMaster and co-workers investigated the influence of Si- or W- doping on DLC coating performance finding a clear correlation between their behaviour in nano- and micro-impact tests and their resistance to sand erosion [28]. The test has also revealed differences in cracking between technical ceramics, with focussed-ion-beam milled sectioning through nano-impact craters revealing sub-surface intergranular cracking on alumina and sub-surface transgranular cracking on MgO-partially stabilised zirconia (PSZ) [20]. Václavek and co-workers used the technique to reveal differences in crack resistance between CNC-machined and hand machining on a range of borosilicate glasses [30].

A more direct way to experimentally simulate the stochastic multiple contact nature of erosion is to perform repetitive controlled impacts at different locations on the sample surface. A novel test technique (randomised impact testing) has been developed to do this for the first time, where sample stage movement between impacts enables each impact to be at a new position [31]. Figure 1 (a) schematically illustrates the principle of operation on a TBC. As an example, figure 1(b) shows the statistical distributions taken from 500-impact tests that were performed with a spheroconical indenter of 25 μm end radius on a gadolinium zirconate thermal barrier coating, with three different sizes of test area. The surface after the test within 1 mm^2 is shown in figure 1 (b). For these tests a rectangular distribution was used where there was an equal probability of the next impact being anywhere within the set region. The method provides the opportunity to follow impact-by-impact how the surface degradation develops, enabling the

interaction between the damage created by individual impacts on subsequent damage to be investigated in detail by changing test conditions, in this case by increasing/reducing the size of the test area.

In this study, we have investigated the impact behaviour of two EB-PVD ceramic TBC systems (yttria stabilised zirconia and gadolinium zirconate) and two glasses (fused silica and BK7) as model systems to investigate the potential of the new test method. The thermal barrier coatings are in use in gas turbines in commercial jet engines. The TBCs have a complex columnar microstructure with pyramidal tops and appreciable inter- and intra-column porosity. The glasses are well-characterised bulk materials, with no microstructure/porosity, low surface roughness and are mechanically homogeneous but brittle. Fused silica is known as an "anomalous" glass whose deformation involves significant densification and the borosilicate glass BK7 as a "normal" glass that deforms primarily through shear flow. These differences in deformation have been shown to influence the crack systems that develop in a quasi-static indentation contact with sharp indenter [32-35].

In this work, we have aimed to (i) validate the new test method to create damage representative of erosion with spatially distributed controlled impacts (ii) investigate the sensitivity of test metrics (residual depth, coefficient of restitution and kinetic energy lost) obtained from analysis of instantaneous depth vs. time data from each impact to provide evidence of transitions in damage mechanisms (iii) compare damage mechanisms in repetitive tests at the same position (iv) investigate how the properties of the model materials (mechanical properties, surface roughness, crack morphology) affect the damage mechanisms in spatially distributed impact tests where the extent of overlap between impacts was modified by changing the number of impacts (50-500) and/or size of the test area (0.01-1 mm^2).

2. Experimental

EB-PVD yttria stabilised zirconia (7YSZ) coating systems were produced with 180 μm 7YSZ top coat on aluminised Ni-Cr alloy (Nimonic 75) and sapphire substrates. EB-PVD gadolinium zirconate (GZO) coating systems were produced with a 175 μm top layer, 25 μm 7YSZ sub-layer on aluminised Ni-Cr alloy (Nimonic 75) and alumina substrates. The NiAl bond coat was deposited by CVD and the top coat by EB-PVD using a Von Ardenne EBE150 coater. Micro-indentation tests were performed with a calibrated diamond indenter with 20 μm end radius and 90° cone angle at 1-10 N using a dual-loading head NanoTest Vantage (Micro Materials Ltd., Wrexham, UK) with 10 s loading, 10 s hold at peak load and 10 s unloading. There were 5 repeat tests at each load.

Surface roughness of the TBCs was determined with Gwyddion software (v. 2.54) from line scans of confocal microscopy (Olympus LEXT) images. The mean and standard deviation of the R_a surface roughness from 10 line scans over 640 μm of 7YSZ and GZO were (1.4 ± 0.1) μm and (0.9 ± 0.3 μm) respectively. The BK7 and fused silica glasses had mirror-polished optical finish (R_a <1 nm, determined by profilometry with a 5 μm diamond probe, NanoTest Vantage).

Nano- and micro-impact tests were performed with a dual-loading head NanoTest Vantage. In the test a diamond indenter is withdrawn to a set distance above the sample surface and then rapidly accelerated to produce a high strain rate impact event. The impact energy and effective impact force can be controlled by varying the static load and/or the accelerating distance. For repetitive impact tests, once the probe has come to rest it is retracted and reaccelerated to produce a set number of repetitive impacts at the same position on the surface. Repeat micro-impact tests at the same position were performed at a range of applied loads using a calibrated spheroconical diamond probe with 25 μm end radius and 90° cone angle impacting at 90° to

the surface accelerating from 50 μm above the initial coating surface. The test duration was 200 s with 1 impact every 4 s, resulting in 50 impacts in total. There were 3 repeats at each load which were separated by 250 μm. The loads used in the repetitive impact tests on the TBCs were 500, 1000, 1500, 2000, 2500 and 3000 mN and for the glasses the loads were 50, 250, 500, 750 and 1000 mN.

Randomised (statistically distributed) micro-impact tests at 90° were set up with a programmed number of statistically distributed impacts within a specified region X-Y centred around a point. A rectangular distribution was used in every test, such that there was equal probability of impacting anywhere within the test region. The tests were performed at 500 mN and accelerating distance of 50 μm using the same spheroconical probe used for the repetitive impacts at the same position. 50-impact tests within a 100 μm x 100 μm region were performed on BK7, 7YSZ and GZO. 500 impacts within 250 μm x 250 μm, 500 μm x 500 μm and 1 mm x 1 mm were performed on GZO. 200 impacts within 500 μm x 500 μm were performed on 7YSZ. Tests of 50, 150, 250 and 500 impacts within 1 mm x 1 mm were performed on both glasses. Tests with 50 impacts were also performed with lower impact energy on 7YSZ and BK7 glass within a 100 μm x 100 μm region with 100 mN and accelerating distance of 13 μm. These nano-impact tests were performed with the same indenter as the micro-impact tests but used the low-load head of the dual head NanoTest Vantage system. The experiments are summarized in Table 1. The same 25 μm probe was used for all the micro-impact tests. After the tests its geometry was rechecked by spherical indentation to confirm that no discernible tip wear had occurred during the tests.

Table 1. Summary of randomised impact experiments

Sample	Impact load (mN)	Accelerating distance (μm)	Number of impacts	Test area (mm^2)
7YSZ	100	13	50	0.01
7YSZ	500	50	50	0.01
7YSZ	500	50	200	0.25
GZO	500	50	50	0.01
GZO	500	50	500	0.0625, 0.25, 1
BK7	100	13	50	0.01
BK7	500	50	50, 150, 250, 500	1
FS	500	50	50, 150, 250, 500	1

Experiments were also performed on the two glasses with controlled spacing between adjacent impacts. The tests were at 500 mN and 50 μm accelerating distance, with rows of 10 impacts spaced 5-100 μm apart and adjacent rows spaced 100 μm apart. On BK7 glass experiments were also performed with 10 tests spaced 120-200 μm apart and adjacent rows spaced 200 μm apart.

Microscopic analysis of the impact damage using a combination of optical, Laser Scanning Confocal Microscopy (Olympus LEXT) and imaging by scanning electron microscopy (Tescan Vega 4) in back-scattered electron mode (BSE SEM) was supplemented by quantitative analysis of depth vs. time data for each impact (maximum depth, residual depth, kinetic energy loss, coefficient of restitution). Figure 2 shows a depth vs. time and velocity vs. time for a typical impact experiment. The grey area marks the region where the indenter and sample are in contact. The individual impacts were analysed in the instrument software to determine the

contact point, the maximum (h_{max}) and residual depths (h_{res}), impact velocity V_{in} and rebound velocity V_{out}. From these the coefficient of restitution (e) and kinetic energy (KE) absorbed were determined. The contact position (h = 0) was defined as the point of maximum velocity (V_{in}). The indenter penetrates the sample to a maximum depth, h_{max}. V_{out} is the maximum rebound velocity reached before the indenter leaves the surface, at h_{res}. The kinetic energy lost during impact is determined from

$$KE \text{ loss} = \tfrac{1}{2}\, m\nu_{in}^2 - \tfrac{1}{2}\, m\nu_{out}^2 \qquad \text{[Eqn. 1]}$$

The effective mass of the loading head was determined by calibration following the approach detailed in Constantinides et al [36]. The coefficient of restitution, e, is defined as

$$e = |\, \nu_{out}/\nu_{in} \,| \qquad \text{[Eqn. 2].}$$

and is a measure of the elasticity of the impact. There is a relationship between the coefficient of restitution and kinetic energy lost so that [36] the % kinetic energy dissipated in the impact is defined by

$$\%\text{ energy dissipation} = 100 \text{ x } (1 - e^2) \qquad \text{[Eqn. 3]}$$

so that for an elastic impact with zero energy loss e = 1.

3. Results

3.1 Repetitive impact tests at the same position

The mechanical properties determined from microindentation tests on the thermal barrier coatings are shown in figure 3. The 7YSZ was harder and stiffer than GZO. Both TBCs typically showed a gradual increase in depth with number of impacts in the repetitive 500 mN impact tests at the same position. Similar behaviour was found for higher impact loads on 7YSZ

but in some of the tests there were discontinuities at higher load for GZO. Figure 4 shows the surfaces of GZO and 7YSZ after repetitive tests at 1 N. For both TBCs the dominant deformation is compaction, with some cracking at the periphery of the crater. Debris was found within the impact crater in some of the tests on GZO but this was not observed for 7YSZ. The initial and final impact depths were greater for GZO.

Illustrative test results to show the load dependence of the evolution of impact depth with number of impacts on FS and BK7 are shown in figure 5 (a,b). There is a strong load dependence with the depth only remaining low at the end of the test at 50 mN. At 250 mN there is a "plateau-like" period where the increase in depth with each successive impact is relatively low before an abrupt displacement step which occurred after 7 impacts on fused silica and 17 impacts on BK7 in these tests. By 500 mN the plateau period is reduced and it is absent at ≥750 mN. Figure 5(c,d) shows example impact craters on BK7 at 50 mN and 500 mN. At 50 mN there was radial cracking with some slight chipping outside the impact periphery. The SEM image reveals brittle response dominated by extensive chipping outside the impact crater and micro/sub-micro sized debris around the edge of the crater at 500 mN, which obscured any radial cracking. Similar behaviour was observed for all impacts at ≥250 mN. Both glasses showed similar behaviour in the tests. The initial impact depth (depth after first impact) was slightly lower for fused silica (figure 5 (e)) but with continued impacting BK7 was generally slightly more resistant so that final depths were lower for BK7, at least to 750 mN (Figure 5 (f)).

3.2 Spatially distributed impact tests

To illustrate the effect of the impact number within a defined area, 50-impact tests at 500 mN were performed on GZO, 7YSZ and BK7 glass within 0.01 mm^2 areas. The distributions used and the evolution in the residual depth with number of impacts from these tests are shown in

figure 6(a,b). Due to the relatively large contact size compared to the test region within a few impacts the test area was rapidly covered by multiple impacts. There were clear differences in damage progression between the three samples. Although the residual depth on BK7 was initially lower there was a transition to more severe damage after around 10 impacts. A similar transition did not occur in a 100 mN test on the BK7 glass within a 0.01 mm^2 region (also shown in figure 6 (b)). The impacts were close to elastic and there was no damage progression through the test. Similar results were obtained on 7YSZ at 100 mN (figure 6 (b)).

The effect of test area is investigated and the results show reduced interaction within a larger area. The impact depths at the start of the 500 mN tests on the TBCs were larger than on BK7. There was no clear upward trend in impact depth for YSZ but a gradual increase in depth with continued impacts was seen for GZO (figure 6 (b)). The gradual impact damage on GZO was investigated by performing longer 500-impact tests over larger areas so that the influence of region area could be studied. The impact area was varied between 0.0625-1 mm^2 using the distributions shown in figure 1(a). Within an area of 1 mm^2 many impacts on GZO occur on new regions of the surface so individual isolated impacts can be seen after the test (figure 1 (b) and 7 (a)). Individual impacts were also clearly observed after a 200-impact test on 7YSZ within a 500 μm x 500 μm area (figure 7 (d)). As the test area is reduced the interaction between impacts increases and on GZO the surface is progressively broken into smaller sized debris. No non-impacted regions remain visible within the test area and only the compaction due to the final few impacts can be seen (figure 7 (b,c)).

The variation in residual depth, kinetic energy lost and the coefficient of restitution from each impact provide more detailed information about the damage progression. On the glasses, experiments were set up within 1 mm^2 regions and the number of impacts varied between 50 and 500. Optical images of the surface after these tests are shown in figure 8 (fused silica) and figure 9 (BK7). With only 50 impacts, the average separation between neighbouring impacts

was sufficiently high that there was limited interaction between them. With continued impacts, the interaction between impacts increases resulting in a transition to a more severe wear mode. The damage was more severe on BK7 although the general trends with increasing impacts were the same for both glasses. The variation in the residual depth with the number of impacts in 50-500 impact tests is shown in figure 10(a) for fused silica and figure 10(b) for BK7. Figure 11 shows a comparison between fused silica and BK7 in 500 impact tests for (a) residual depth (b) *KE* absorbed (c) coefficient of restitution. Figure 11 shows that there was a clear transition after around 250 impacts on BK7 which was not observed for fused silica although occasional impacts higher depths and *KE* loss occurred ≥380 impacts. Figure 12 shows illustrative depth vs. time data for two impacts on BK7, one before (impact 202) and one after (impact 305) there was transition to more severe damage accumulation. Although after the transition several impacts were very similar to those before the transition some showed decreased elastic recovery, as illustrated in the figure. After ~250 impacts on BK7 the coefficient of restitution was generally lower after ~250 impacts since several impacts had higher V_{in} without as significant corresponding rises in V_{out}.

To study the interaction between two impacts without complexity from subsequent impacts, experiments were performed with controlled spacing between adjacent impacts. These revealed marked differences in behaviour for the two glasses. Laser scanning confocal microscopy images of the controlled spacing experiment on fused silica (a) normal (i.e. white light) (b) green light are shown in figure 13 (a,b) with higher magnification images of impacts 60 and 70 μm apart shown in figure 13 (c,d). Figure 14 shows SEM images of controlled spacing experiments on BK7 (a) 5-100 μm spacing array (b) impacts 120 and 140 μm apart (c) higher magnification image of impacts with 120 μm spacing. The images in figures 13 and 14 reveal a critical separation distance exists below which there was more extensive interaction between impacts but this distance varied by a factor of two between the two glasses. Cracks between

some impacts appeared to join up, or nearly join up, when the spacing was reduced to 60 μm for fused silica (figure 13(c,d)) and to 120 μm for BK7 (figure 13(b)). Closer inspection showed that these cracks generally did not join up at the surface for BK7 but they did appear to for fused silica. Imaging under green light (figure 13(b,d)) revealed additional sub-surface cracking more clearly. When the spacing was reduced to <20 μm significantly more damage was produced on both glasses, which resulted in more extensive lateral cracking on BK7.

4. Discussion

In these tests on four model materials, the new test method has been employed to create damage representative of erosion with spatially distributed, controlled energy impacts and the behaviour compared to the damage mechanisms in repetitive tests at the same position. How the properties of the model materials (specifically their mechanical properties, surface roughness, crack morphology) combine to control the damage mechanisms in the spatially distributed tests was investigated by modifying the extent of overlap between impacts and damage accumulation through varying the number of impacts and/or the size of the test area.

4.1 General features in single impact – influence of mechanical properties and surface roughness

Due to their surface roughness, together with some inter- and intra-columnar porosity, EB-PVD TBCs are challenging to test reliably by indentation testing. For this reason, they are usually polished (to remove the tops of the columns and create a much smoother surface) before indentation testing. The hardness of well-polished 7YSZ has been determined previously in nano- and micro-indentation tests with sharp pyramidal Berkovich [5] and Vickers [37]

indenters. The data show a size effect in hardness due to the columnar structure where, as the load increased, the indentation size increased to span several columns and there was column buckling. Hardness of individual polished columns was 14 GPa at 100 mN decreasing to 2.4 GPa at 3 N, where the indentation size spanned several columns. In the current study, the micro-indentation tests were performed on the as-deposited (non-polished) TBCs as the surface could not be modified before impact testing. Lower values were found, but these varied relatively little over a wide depth range (mean values between 1-10 N were H = 1.9 GPa, E = 84 GPa for 7YSZ and H = 1.5 GPa, E = 64 GPa for GZO). Hardness was lower at smaller depth due to the greater effect of the high surface roughness. Elastic modulus, being a far field effect, was relatively less affected by this roughness. The elastic modulus of 7YSZ is close to the value of 77 GPa reported by Kim and Heuer on a well-polished EB-PVD 7SYZ in Vickers indentation at 1 N [37]. The hardness at 4 N was 2 GPa, which was close to the 2.4 GPa reported in micro-indentation data on a highly polished 7YSZ with a Berkovich at 3 N [5].

In single impact, both TBCs show a similar deformation mechanism dominated by compaction – squashing down the high surface roughness with some cracking of the tops of the columns at the periphery of the impact crater where the tensile stresses are greater. GZO with its lower hardness and stiffness exhibits larger impact craters than 7YSZ. Both TBCs showed larger impact craters than either glass consistent with their significantly lower hardness due to the high roughness and inter- and intra-columnar porosity.

The contrasting differences in mechanical properties (e.g. H/E ~0.02 for the TBCs, H/E >0.08 for the glasses), surface roughness and structure between the TBCs and the glasses are reflected in differences in their cracking behaviour. Initial impact depths varied in the order GZO > 7YSZ >> BK7 > fused silica. The resistance to initial impact correlates with differences in their H^3/E^2 values (fused silica = 0.15 GPa; BK7 = 0.042 GPa; 7YSZ = 0.001 GPa; GZO = 0.0008 GPa) which have been considered as measures of their load-carrying capacity [38], and in some

cases, with H/E, as predictors of likely erosion resistance [3, 38]. Both glasses show more brittle behaviour than the TBCs with less compaction due to their higher H/E. Within the two glasses, there are clear differences in the predominant type of crack systems developed that are related to differences in their mechanical properties and structure. As an anomalous glass with an open structure, fused silica deforms by predominantly densification whilst the normal glass BK7 deforms by conventional shear [32-35]. The mechanical properties of the glasses are H = 9.2 GPa, E = 72 GPa for fused silica; H = 6.2 GPa, E = 75 GPa for BK7. These differences influence the crack systems that develop. Rouxel and co-workers studied the influence of H/E and Poisson's ratio (ν) on the driving force for ring/cone cracking and sub-surface lateral cracking on indentation of glasses with sharp indenters [32,33], generating maps of regions where each crack type could be expected to occur if fracture toughness is not too high. When $\nu < 0.18$, the stress near the contact edge at the surface is positive (tensile) so that ring/cone cracks are likely to form during loading. In contrast, the stress for sub-surface lateral cracking is negative during loading when $\nu < 0.2$ but becomes positive on unloading, especially at higher ν, and lateral cracking can be expected on unloading [32]. Since fused silica has $\nu = 0.17$ and $H/E = 0.13$ and BK7 has $\nu = 0.21$ and $H/E = 0.08$ they are in different regions of Rouxel's maps. The lower Poisson ratio and higher H/E in fused silica results in cone cracking whilst the higher Poisson ratio and lower H/E in BK7 in lateral/radial. Yoshida [34] used a photo-elastic technique to directly measure the stresses developed. High tensile stress was found when indenting fused silica at 3 N with a spherical indenter with 50 μm radius, but in contrast on soda-lime glass ($\nu = 0.22$) the tensile stress moved towards the bottom of the plastic zone, providing the driving force for radial cracking. With support of data from Vickers indentation, Barlet and co-workers developed a map showing transitions between regions for (i) cone and median cracking at low ν (ii) median and radial cracking at intermediate ν and (iii) lateral and radial cracking at high ν [35].

The impact experiments with controlled spacing (figures 13 and 14) also show differences in crack morphology between the anomalous and normal glass under spherical impact. For fused silica, the laser scanning confocal microscopy imaging showed predominant cone cracking with some chipping and the imaging under green light revealed “spinning” cracks. The line between the impacts is due to the interaction between adjacent cone cracks. Radial/lateral cracking predominated for BK7. The deformation in spherical impact for the two glasses can be compared to that previously reported in indentation and impact tests with sharper indenters, and in non-depth sensing macro-scale impact tests with larger angular particles. Low load nano-impact tests on fused silica with sharper probes did not observe any ring/cone cracking [40]. Impact tests with Berkovich indenter did not produce cracks at a crater area where a quasi-static indentation would. Cube corner nano-impact produced radial cracking with some impacts showing chipping. Bruns and co-workers noted that, in quasi-static indentation, the Berkovich indenter activates multiple crack systems with a cube corner indenter producing radial and chipping in 90% of indents [41]. Chaudhri [42] using a high-speed camera reported that, in high-speed impact, spherical indenters (e.g. 1 mm radius) generated Hertzian cone cracking in fused silica but conical indenters (90° cone with R~10 μm) generated sub-surface median cracks. Waxman and co-workers reported that angular sand particles produced extensive lateral chipping on BK7 [43-45].

4.2 Repetitive impact in same position - effect of high-stress low-cycle fatigue

Repetitive impact at the same position effectively results in a high-stress low-cycle surface fatigue test. When 7YSZ was repetitively impacted at the same position, there was a gradual damage progression during the tests. Increasing the impact load increased the extent of surface damage but without an obvious change in mechanism, which was predominantly compaction

within the crater and cracking around the periphery. There was more impact damage on GZO. It behaved similarly but with more complex behaviour in some tests at 1 N and above, with the presence of debris found within the impact crater consistent with its lower fracture toughness. The fracture toughness of 7YSZ is relatively low, around 0.1-0.5 MPa $m^{1/2}$ [46], and Mahade and co-workers noted that the fracture toughness of GZO was around half of that of 7YSZ [47].

Typical impact results from all four samples at 500 and 1000 mN are shown in figure 15(a.b). In contrast to the gradual increase in depth for the TBCs, the glasses showed strongly load-dependent responses with the impact depth remaining low throughout the tests at the lowest load and abrupt displacement bursts occurring after several impacts at higher loads. The development of a "plateau depth" where the depth stabilises after a number of impacts as plasticity is exhausted, followed by one or more abrupt displacement bursts is typically observed on brittle materials when repetitive impact tests are performed at the same position. Displacement bursts have been reported in blunt (spherical) impact of bulk ceramics [19], and in sharp (cube corner) impact on fused silica [40]. They occur due to lateral cracking and the linkage of crack systems under the impact zone that develop under repetitive contact to cause material removal. Jennett and Nunn have shown that these displacement bursts are associated with increased energy absorption [40] and Crtvrlik and co-workers have shown that they are accompanied by large bursts of acoustic emission [20].

For both glasses, damage mechanisms under repetitive contact were more complex than under single impact. A load-dependent transition to damage with lateral cracking/chipping and subsequent further cracking and generation of sub-micron sized debris at crater edge was found in the repetitive tests at ≥250 mN. The presence of multiple material removal processes is supported by the changing impact wear rate after the initial displacement burst. Lateral chipping and extensive sub-micron sized debris around the periphery of the impact crater has

been typically found in micro-impact tests with spherical indenters with similar end radii, e.g. on hardmetals and nitride coatings on hard metals [21].

Although initially more resistant to single impact (consistent with its higher H^3/E^2), fused silica was generally slightly more susceptible to continued impact damage than BK7 glass in the multiple impact tests at the same position. This may, in part, be related to differences in their fracture toughness since K_{IC} for fused silica (~0.68 MPa $m^{1/2}$ [41], 0.74 MPa $m^{1/2}$ [48]) is lower than that on BK7 (0.85 MPa $m^{1/2}$ [49], 1.03 ± 0.05 MPa $m^{1/2}$ [49]).

4.3 Randomised impact - influence of crack morphology and coating microstructure

The novel test method provides a new opportunity to investigate how solid particle impact damage of the surface proceeds impact-by-impact and how this relates to material removal. Post-test microscopy and analysis of individual impact depth-time data provide complementary approaches to the evaluation of surface degradation. Metrics from depth-time data are "in situ" measurements that can provide precise information on how damage accumulation/and the exact number of impacts required, for example in wear-mode transitions from mild to severe.

The behaviour in the short 50-impact tests within 0.01 mm^2 showed similarities to the repetitive impact tests at the same position, presumably due to the high degree of overlap between many of the impacts. BK7 showed an initially low impact depth before undergoing a transition to a more severe wear regime. The damage was more gradual on GZO and 7YSZ, as illustrated in SEM images from longer tests with greater spacing, and the impacts on the TBCs can be overlapping without triggering a dramatic transition. The columnar structure in EB-PVD TBCs provides a measure of damage tolerance by partially stopping the crack propagation across columns, a well-known phenomenon observed in erosion testing [6]. The poorer performance for GZO is consistent with its higher erosion rate [50] and lower fracture toughness [47].

The gradual damage process on GZO was investigated in more detail by performing 500-impact tests over larger test areas. The results (figure 7(c)) reveal that the low fracture toughness of the GZO results in continual cracking progressively destroying the surface such that micron scale debris covered almost the entire test area, with the exception of the compaction from the last few impacts. The covering up of previous impacts with this fine debris is consistent with the presence of debris in the impact craters in some repetitive impact tests at the same position at ≥1 N.

Although the impact resistance of fused silica was generally slightly worse in the repetitive tests at the same position, in the randomised impact and controlled impact spacing tests it was considerably better than BK7.

The differences that emerge during the distributed impact tests on BK7 and fused silica are a result of a transition to more severe chipping after a "critical damage threshold" (or critical impact density) is reached. The radial-lateral crack system in BK7 reaches this threshold after a smaller number of impacts, due to the larger distance at which impacts can influence other impacts (when the lateral cracks join up there is extensive chipping and material removal). The critical threshold is higher for fused silica, as the cone cracks need to be closer together (lower critical interaction spacing) before the damage from one starts to affect another, and consequently the cone cracking is less efficient in causing the transition to the more severe wear. This is consistent with reports of better erosion resistance for fused silica. Waxman and co-workers [43-45] reported larger damage footprints for BK7 than fused silica in erosion tests with sand and spherical microparticles. For a given incoming kinetic energy there were significantly greater damaged areas for BK7 than FS in tests with angular sand particles [45].

The absorbed kinetic energy gradually increases with number of impacts on both glasses due to damage creation within the test area. At the transition to more severe wear there is a greater

increase in magnitude and scattering of absorbed *KE*. The absorbed kinetic energy is higher on BK7 since (i) there is more plasticity on BK7 and (ii) creating the more extensive radial-lateral crack system absorbs more impact energy than the cone cracking on fused silica.

There is a clear difference in the coefficient of restitution between the two glasses with fused silica showing the higher (more elastic) behaviour consistent with its higher dynamic H/E. Applying relationships developed by Constantinides [36] from an analysis of Andrews *et al* [51] for sharp impact suggests that the coefficient of restitution should be proportional to $(H/E)^{1/2}$. A generally higher coefficient of restitution for BK7 over FS was also found in high-speed camera analysis of sand particle impacts by Waxman *et al* [45].

The transition did not change the coefficient of restitution in most impacts, however, for some impacts it was significantly lower. As an example, the coefficients of restitution for the two impacts on BK7 shown in figure 12 were 0.49, for the impact before the transition, and 0.23 for the impact after it. The increased variability in the coefficient of restitution is due to the onset of the more severe cracking with chipping and material removal. This causes more variability in V_{in} and V_{out} and hence in e. On BK7, the severe cracking causes differences in V_{in} due to topographical changes (i) higher V_{in} when impacts occur on already heavily fractured regions (ii) lower V_{in} when impacts occur in regions where there is uplifted impact debris. These result in differences in V_{out}. Impacts in regions with uplifted debris have lower V_{out}, presumably due to greater fracture, resulting in lower e. On fused silica the transition to severe wear does not occur to the same extent and so the same variability in V_{in} was not observed, although there was lower V_{out} in some impacts towards the end of the 500 impact tests, presumably due to increased fracture.

Despite this, the kinetic energy loss was found to be generally a more sensitive marker of fracture than the coefficient of restitution. The lateral fracture in BK7 results in more variable kinetic energy absorption.

The number of impacts needed to produce a transition to a more severe wear mode on BK7 was a function of their separation and the impact energy. In the repetitive tests at the same position at 500 mN, only 3-4 impacts were required before there was a transition to a more rapid impact wear. In the 50 impact 500 mN tests within 0.01 mm^2 area, the residual depth started to increase after 10 impacts whilst within 1 mm^2 around 250 impacts were required. This difference is related to lateral cracking and the joining up and extension of crack networks. Lawn and co-workers noted that the cumulative effect of lateral cracks spreading sideways from the deformation zone that tend to cause chipping has a major influence on the erosion properties of ceramics [52]. Similar load and spacing-dependent transitions on BK7 have also been observed in nano-scratch tests with a sharp Vickers indenter [53]. Above a critical load, the damage caused by the first scratch resulted in dramatically increased material removal when a second parallel scratch was made within 60 μm or less of the first scratch, but below the critical load threshold the scratches could be much closer without this occurring.

The four materials tested have different “critical interaction thresholds” where damage generated from one impact affects the damage accumulation and subsequent erosion rate. Crack morphology and fracture toughness have differing importance in the erosion rate of the glasses and TBCs respectively. For the glasses, crack morphology is important and the randomised impact test is more sensitive to this than the repetitive impacts at the same position. In comparison to the lateral, radial and cone cracking in the glasses, the TBCs undergo more compaction and cracking localised to the periphery of the impact where the tensile stresses are highest, with the columnar structure of the TBCs providing a measure of crack retardation.

The spatially-distributed impact test methodology shows promise for rapid effective screening of the impact/erosion resistance of novel coating compositions. It has potential applications beyond erosion simulation. For example, creating surfaces by controlled spatially-distributed application of impacts could simulate processes such as shot peening, where compressive residual stresses are introduced in the surface of a component and may also have some application to micro-pitting. Although the tests described in this work all involved 90° impacts at room temperature, it is also possible to control the impact angle, alter the distribution of the impact loads during the randomised impact tests, and perform tests at elevated temperature to simulate high-temperature erosion.

5. Conclusions

A novel randomised nano-/micro- impact test for simulating particle impact in erosion has been developed where a specific number of statistically distributed impacts with defined energy occur sequentially within the test area. Tests were performed on four model materials systems, two TBCs with high surface roughness and complex microstructure, and two amorphous glasses with higher hardness and very low surface roughness. The tests provide the opportunity to investigate how solid particle impact damage of the surface proceeds *impact-by-impact,* and how this damage accumulation relates to material removal. Analysis of the depth-time curves of each individual impact provides quantitative metrics that can yield detailed information on how damage accumulates, and the number of impacts or impact density required for mechanistic transitions from mild to more severe impact wear with increasing damage.

Trends in erosion resistance were reproduced in the randomised impact tests, with GZO less impact resistant than 7YSZ, and BK7 significantly worse than fused silica. The randomised impact test identified critical interaction thresholds where damage generated from one impact

affects the subsequent rate of impact wear. Differences in these thresholds highlight the importance of crack morphology on erosion resistance of glasses. With the radial-lateral cracking on BK7, impacts interact further apart resulting in a more rapid rate of surface erosion than for fused silica, where cone cracking dominates. Impact-induced damage on the TBCs proceeds more gradually and fracture toughness has a stronger influence.

6. Acknowledgements

Support from Innovate UK under Smart Award project #10020751, High temperature tools for designing sustainable erosion resistant coatings, is gratefully acknowledged. We would also like to acknowledge the assistance of Dr Peter Woolliams (National Physical Laboratory, UK) with the laser scanning confocal microscopy.

7. References

1. I.M. Hutchings, Ductile-brittle transitions and wear maps for the erosion and abrasion of brittle materials, J. Phys. D: Appl. Phys. 25 (1992) A212.
2. H. Wensink, M.C. Elwenspoek, A closer look at the ductile-brittle transition in solid particle erosion, Wear 253 (2002) 1035-1043.
3. S.J. Bull, Using work of indentation to predict erosion behaviour in bulk materials and coatings, J. Phys. D: Appl. Phys. 39 (2006) 1626-1634.
4. T. Zisis, N.A. Fleck, The elastic-plastic indentation response of a columnar thermal barrier coating, Wear 268 (2010) 443-454.
5. R.G. Wellman and J.R. Nicholls, Nano and Micro indentation studies of bulk zirconia and EB PVD TBCs, Surf. Coat. Technol. 176 (2004) 253-260.
6. R.G. Wellman and J.R. Nicholls, A review of the erosion of thermal barrier coatings, J. Phys. D: Appl. Phys. 16 (2007) R293-R305.
7. R.G. Wellman and J.R. Nicholls, A mechanism for the erosion of EB PVD TBCs, Mater. Sci, Forum, 369-372 (2001) 531-538.
8. A.G. Evans, N.A. Fleck, S. Faulhaber, N. Vermaak, M. Maloney, R. Darolia, Scaling laws governing the erosion and impact resistance of thermal barrier coatings, Wear 260 (2006) 886-894.
9. X. Chen, M.Y. He, I. Spitsberg, N.A. Fleck, J.W. Hutchinson, A.G. Evans, Mechanisms governing the high temperature erosion of thermal barrier coatings, Wear 256 (2004) 735-756.
10. R.G. Wellman, J.R. Nicholls, Some observations on erosion mechanisms of EB-PVD TBCs, Wear 242 (2000) 89-96.
11. J.R. Nicholls and R.G. Wellman, Erosion and foreign object damage of thermal barrier coatings, Proc. RTO AVT, “The control and reduction of wear in military platforms”, Williamsburg, USA, 2003 published as Nato report RTO-MP-AVT-109-20 (2004).
12. R.G. Wellman, J.R. Nicholls, K. Murphy, Effect of microstructure and temperature on the erosion rates and mechanisms of modified EB PVD TBCs, Wear 267 (2009) 1927-1934.
13. D.R. Clarke, M. Oechsner and N.P. Padture, Thermal-barrier coatings for more efficient gas-turbine engines, MRS Bull. 37 (2012) 891-898.
14. B.D. Beake, Nano- and micro-scale impact testing of hard coatings: a review, Coatings 12 (2022) 793.
15. M. Humood, A. Beheshti, J.L. Meyer, A.A. Polycarpou, Normal impact of sand particles with solar panel glass surfaces, Tribol.Int. 102 (2016) 237-248.
16. D.K. Kim, Y.-G. Jung, I.M. Peterson, B.R. Lawn, Cyclic fatigue of intrinsically brittle ceramics in contact with spheres, Acta Mater. 47 (1999) 4711-4725.
17. F. Guiberteau, N.P. Padture, H. Cai, B.R. Lawn, Indentation fatigue – a simple cyclic Hertzian test for measuring damage accumulation in polycrystalline ceramics, Philos. Mag. A 68 (1993) 1003-1016.
18. K.-D. Bouzakis, A. Siganos, T. Leyendecker and G. Erkens, Thin hard coatings fracture propagation during the impact test, Thin Solid Films 460 (2004) 181-189.

19. R. Bantle, A. Matthews, Investigation into the impact wear behaviour of ceramic coatings, Surf. Coat. Technol. 74-75 (1995) 857-868.
20. B.D. Beake, R. Ctvrtlik, A.J. Harris, A.S. Martin, L. Vaclavek, J. Manak, V. Ranc, High frequency acoustic emission monitoring in nano-impact of alumina and partially stabilised zirconia, Mater. Sci. Eng. A 780 (2020) 139159 (11pp).
21. B.D. Beake, L. Isern, J.L. Endrino, T.W. Liskiewicz, X. Shi, Micro-scale impact resistance of coatings on hardened tool steel and cemented carbide, Mater. Lett. 284 (2021) 129009.
22. B.D. Beake, L. Isern, D. Bhattacharyya, J.L. Endrino, K. Lawson, T. Walker, Nano- and micro-scale impact testing of zirconia, alumina and zirconia-alumina duplex optical coatings on glass, Wear 462-463 (2020) 203499.
23. K.-D. Bouzakis, F. Flocke, G. Skordaris, E. Bouzakis, S. Geradis, G. Katirtzoglou and S. Makrimallakis, Influence of dry micro-blasting grain quality on wear behaviour of TiAlN coated tools, Wear 271 (2011) 783-791.
24. G. Skordaris K.-D. Bouzakis, P. Charalampous, E. Bouzakis, R. Paraskevopoulou, O. Lemmer, S. Bolz, Brittleness and fatigue effect of mono- and multi-layer PVD films on the cutting performance of coated cemented carbide inserts, CIRP Annals - Manuf Tech 63 (2014) 93.
25. G. Skordaris, K.D. Bouzakis, T. Kotsanis, P. Charalampous, E. Bouzakis, B. Breidenstein, B. Bergmann, B. Denkena, Effect of PVD film's residual stress on their mechanical properties, brittleness, adhesion and cutting performance of coated tools, CIRP. J. Manufact. Sci. Technol. 18 (2017) 145-151.
26. B.D. Beake, J.F. Smith, A. Gray, G.S. Fox-Rabinovich, S.C. Veldhuis, J.L. Endrino, Investigating the correlation between nano-impact fracture resistance and hardness/modulus ratio from nanoindentation at 25-500ºC and the fracture resistance and lifetime of cutting tools with Ti1-xAlxN (x=0.5 and 0.67) PVD coatings in milling operations, Surf. Coat. Technol. 201 (2007) 4585.
27. J. Chen, B.D. Beake, R.G. Wellman, J.R. Nicholls, H. Dong, An investigation into the correlation between nano-impact resistance and erosion performance of EB-PVD thermal barrier coatings on thermal ageing, Surf. Coat. Technol. 206 (2012) 4992-4498.
28. S.J. McMaster, T.W. Liskiewicz, A. Neville, B.D. Beake, Probing fatigue resistance in multi-layer DLC coatings by micro- and nano-impact: Correlation to erosion tests, Surf. Coat. Technol. 402 (2020) 126319.
29. L. Ventakesh, S.B. Pitchuka, G. Sivakumar, R.C. Gundakaram, S.V. Joshi, Microstructural response of various chromium carbide based coatings to erosion and nano impact testing, Wear 386-387 (2017) 72-79.
30. L. Václavek, J. Tomáštik, R. Čtvrtlik, Effect of machining on mechanical properties of borosilicate glasses, Powder Metallurgy Progress, 22 (2022) 62-74.
31. UK Patent Application #2217939.4 Surface Testing Apparatus (Erosion) 29/11/22.
32. T. Rouxel, J-I. Jang, U. Ramamurty, Indentation of glasses, Prog. Mater. Sci. 121 (2021) 100834.
33. T. Rouxel, Driving force for indentation cracking in glass: composition, pressure and temperature dependence, Phil. Trans. R. Soc. A 373 (2015) 20140140.

34. S. Yoshida, Indentation deformation and cracking in oxide glass -toward understanding of crack nucleation, J. Non-Cryst. Sol. X 1 (2019) 100009.
35. M. Barlet, J.-M. Delaye, T. Charpentier, M. Gennisson, D. Bonamy, T. Rouxel, C. Rountree, Hardness and toughness of sodium borosilicate glasses via Vickers's indentations, J. Non Cryst. Sol. 417-418 (2015) 66-79.
36. G. Constantinides, C.A. Tweedie, N. Savva, J.F. Smith, K.J. Van Vliet, Quantitative impact testing of energy dissipation at surfaces, Exp. Mech. 49 (2009) 511–522.
37. C.-H. Kim, A.H. Heuer, A high-temperature displacement-sensitive indenter for studying mechanical properties of thermal barrier coatings, J. Mater. Res. 19 (2004) 351-356.
38. K.L. Johnson, Contact Mechanics, Cambridge University Press, London, UK, ISBN: 0-521-34796-3, (1985) p.464.
39. E. Bousser, L. Martinu, J.E. Klemberg-Sapieha, Solid particle erosion mechanisms of protective coatings for aerospace applications. Surf. Coat. Technol. 257, (2014) 165-181.
40. N.M. Jennett, J. Nunn, High resolution measurement of dynamic (nano) indentation impact energy: A step towards the determination of indentation fracture resistance, Philos. Mag. 91 (2011) 1200–1220.
41. S. Bruns, L. Petho, C. Minnert, J. Michler, K. Durst, Fracture toughness determination of fused silica by cube corner indentation cracking and pillar splitting, Mater. Des. 186 (2020) 108311.
42. M.M. Chaudhri, Dynamic fracture of inorganic glasses by hard spherical and conical projectiles, Phil. Trans. R. Soc. A 373 (2015) 20140135.
43. R. Waxman, P. Gray, I. Guven, Particle shape effect on erosion of optical glass substrates, J. Appl. Phys. 123 (2018) 115104.
44. R. Waxman, I. Guven, An experimental and peridynamic study of the erosion of optical glass targets due to sand and sphere microparticles, Wear 428-429 (2019) 340-355.
45. R. Waxman, I. Guven, P. Gray, SPIE Defense and Commercial Sensing Conference, Anaheim, CA, 2017. NASA Technical Report 20170004428.
46. X. Geng, R. Wellman, L. Isern, C. Chalk, Estimation of thermal barrier coating fracture toughness using integrated computational materials engineering, Ceram. Int. 49 (2023) 25788-25794.
47. S. Mahade, N. Curry, S. Björklund, N. Markocsan, S. Joshi, Durability of Gadolinium Zirconate/YSZ double-layered thermal barrier coatings under different thermal cyclic test conditions, Materials 12 (2019) 2238.
48. K.B. Doyle, M.A. Kahan, Design strength of optical glass, Proc. SPIE 5176 Optomechanics 2003, ed. A.E. Hatheway, pp14-25, 2003.
49. G.D. Quinn, J.J. Swab, Adventures and misadventures in applying ASTM standard test method C1421 to measurements of the fracture toughness, K1C, of glasses, Ceramic Engineering and Science Proceedings 37 (2016) 29-44.
50. U. Schulz, A. Nowotnik, S. Kunkel, G. Reiter, Effect of processing and interface on the durability of single and bilayer 7YSZ / gadolinium zirconate EB-PVD thermal barrier coatings, Surf. Coat. Technol. 381 (2020) 125107.

51. E.W. Andrews, A.E. Giannakopoulos, E. Plisson, S. Suresh, Analysis of the impact of a sharp indenter, Int. J. Solids Struct. 39 (2002) 281-295.
52. B.R. Lawn, D.B. Marshall, P. Chantikul, G.R. Anstis, Indentation fracture: Applications in the assessment of strength of ceramics, J. Aust. Ceram. Soc. 16 (1980) 4.
53. W. Gu, Z. Yao, X. Liang, Material removal of optical glass BK7 during single and double scratches, Wear 270 (2011) 241-246.

Figure captions

1. (a) Schematic illustration of the test on a TBC (b) Randomised 500-impact tests within different areas (c) SEM image of the surface of GZO after 500 impacts within 1 mm^2.
2. Typical depth and velocity vs. time data for a single impact.
3. Hardness and elastic modulus of 7YSZ and GZO from microindentation to 1-10 N.
4. BSE SEM images of the impact craters produced by 50 impacts at the same position at 1 N (a) 7YSZ (b) GZO.
5. Repetitive impact tests at same position. Load dependence of the evolution of impact depth with number of impacts on (a) Fused silica and (b) BK7. BSE SEM images of impact craters on BK7 after repetitive impact tests at (c) 50 mN and (d) 500 mN. Load dependence of the initial (e) and final (f) impact depth.
6. (a) Distributions used in randomised 50-impact tests within 0.01 mm^2. (b) Corresponding residual depth data, with results of lower energy tests (100 mN; accelerating distance = 13 μm) on BK7 and 7YSZ also shown.
7. BSE SEM images of (a) GZO surface after 500 impacts (a) within 1 mm^2 (b) within 0.25 mm^2 (c) within 0.0625 mm^2 (d) 7YSZ after 200 impacts within 0.25 mm^2.
8. Randomised impact tests of (a) 50, (b) 150, (c) 250 and (d) 500 impacts with a rectangular distribution within 1 mm^2 on fused silica.
9. Randomised impact tests of (a) 50, (b) 150, (c) 250 and (d) 500 impacts with a rectangular distribution within 1 mm^2 on BK7.
10. Residual depth vs. number of impacts in 50-500 impact tests on (a) fused silica (b) BK7.
11. Comparison between fused silica and BK7 in 500 impact tests (a) residual depth (b) KE absorbed (c) coefficient of restitution.
12. Typical depth vs. time data for impacts on BK7 before (#202) and after (#305) the transition to a more severe damage regime.

13. LEXT imaging of controlled spacing experiment on fused silica (a) normal (b) green light. Higher magnification images of impacts 60 and 70 μm apart under (c) normal (d) green light.
14. BSE images of controlled spacing experiments on BK7 (a) 5-100 μm spacing array (b) impacts 120 and 140 μm apart (c) higher magnification image of impacts with 120 μm spacing.
15. (a) Comparison between samples in repetitive tests at same position (a) 500 mN (b) 1000 mN.

Figures

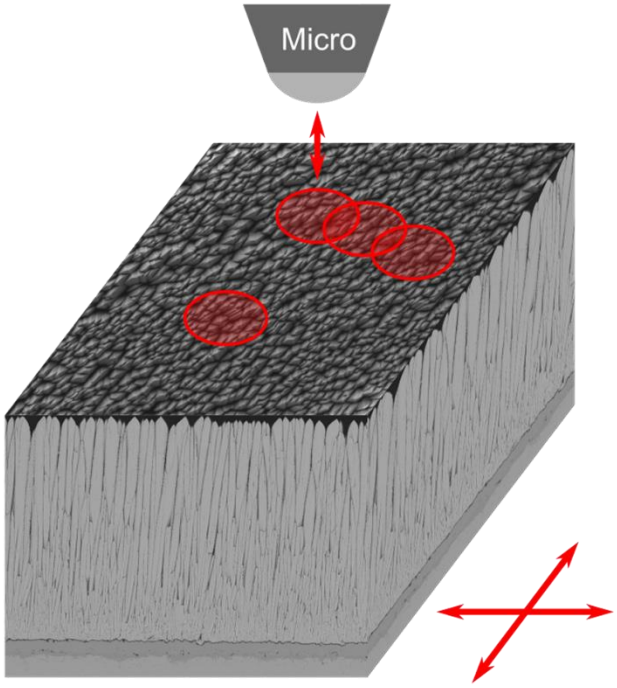

1(a)

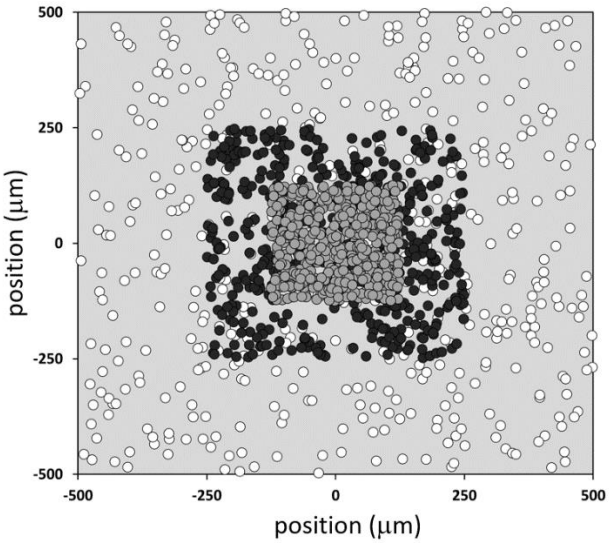

1(b)

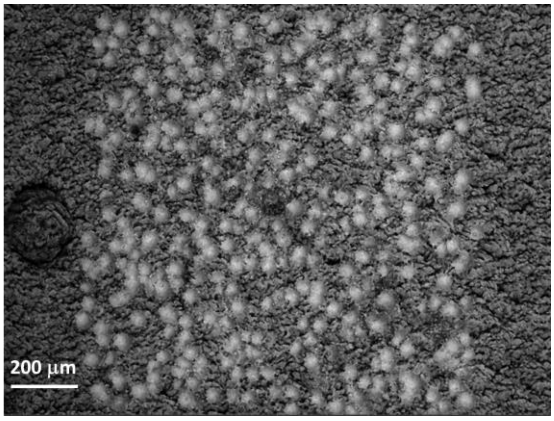
200 μm

1(c)

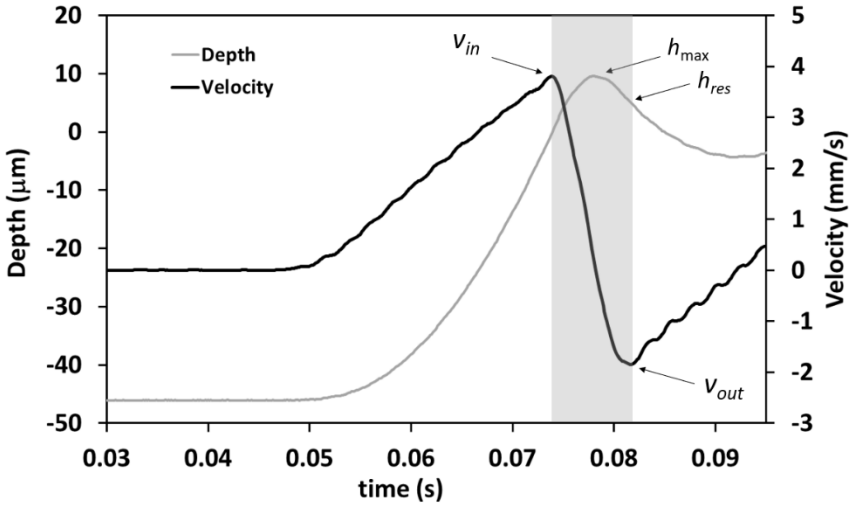
Depth
Velocity
v_{in}
h_{max}
h_{res}
v_{out}
Depth (μm)
Velocity (mm/s)
time (s)
20
10
0
-10
-20
-30
-40
-50
5
4
3
2
1
0
-1
-2
-3
0.03
0.04
0.05
0.06
0.07
0.08
0.09

2

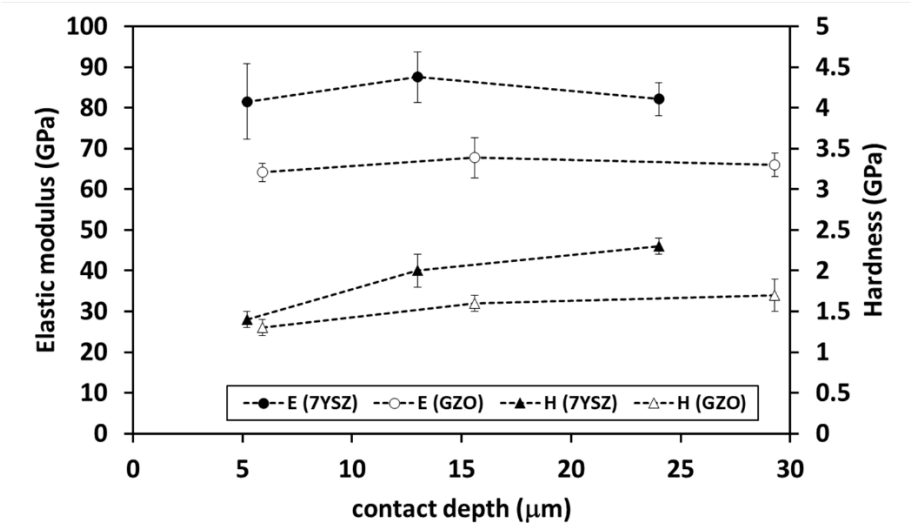
Elastic modulus (GPa)
Hardness (GPa)
contact depth (μm)
E (7YSZ)
E (GZO)
H (7YSZ)
H (GZO)
100
90
80
70
60
50
40
30
20
10
0
5
4.5
4
3.5
3
2.5
2
1.5
1
0.5
0
0
5
10
15
20
25
30

3

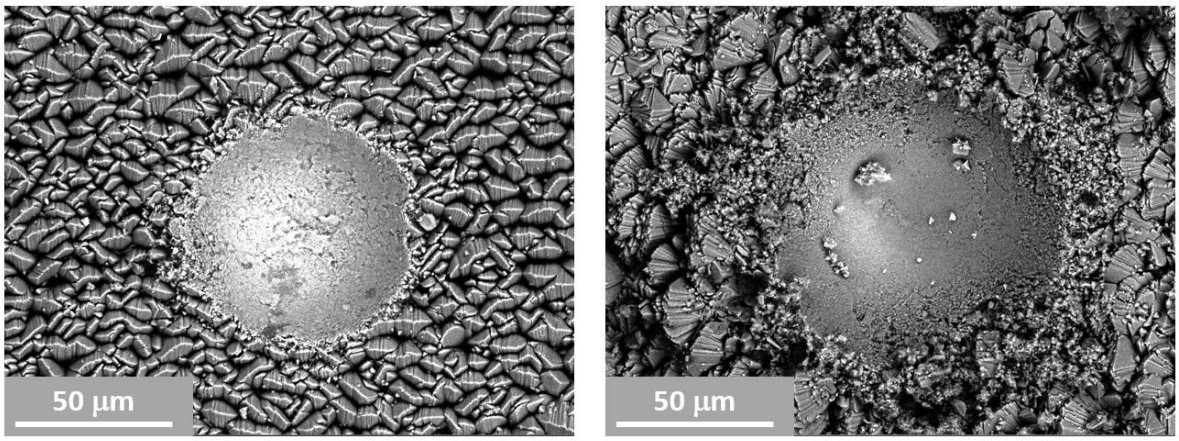
50 μm
50 μm
(a)
(b)

4

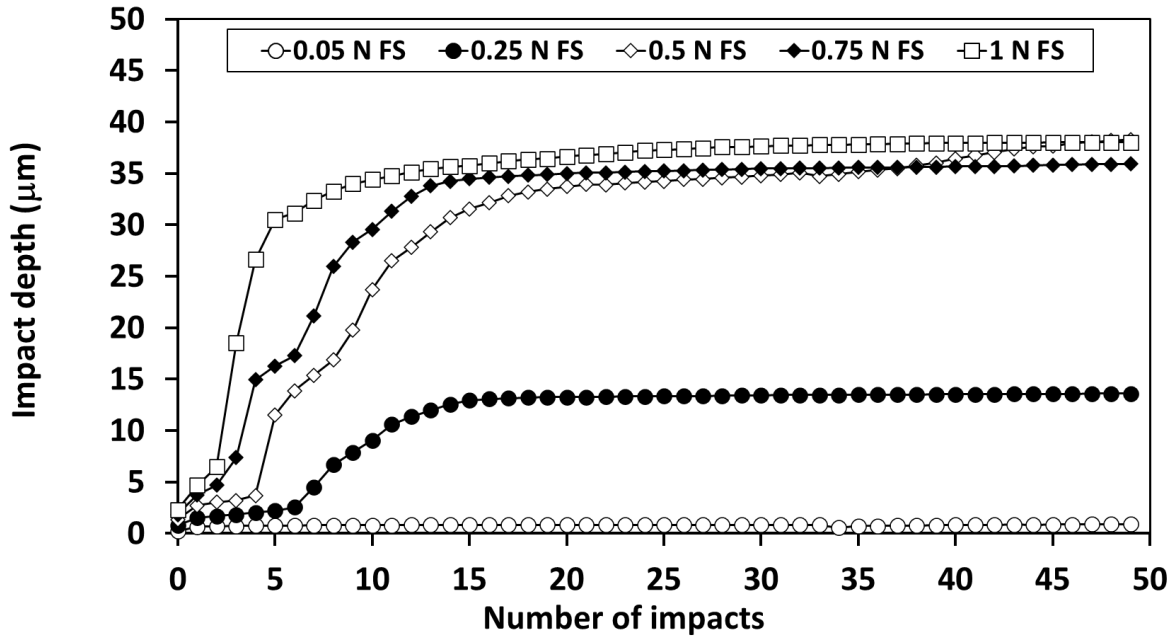
0.05 N FS
0.25 N FS
0.5 N FS
0.75 N FS
1 N FS
Impact depth (μm)
Number of impacts
0
5
10
15
20
25
30
35
40
45
50

5 (a)

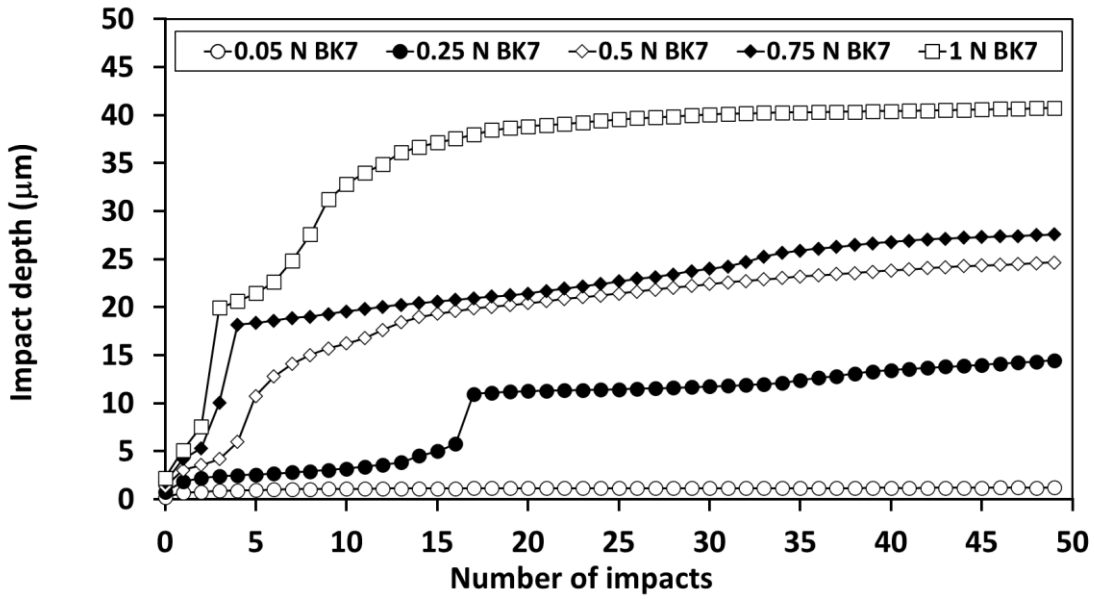
0.05 N BK7
0.25 N BK7
0.5 N BK7
0.75 N BK7
1 N BK7
Impact depth (μm)
Number of impacts
0
5
10
15
20
25
30
35
40
45
50

5 (b)

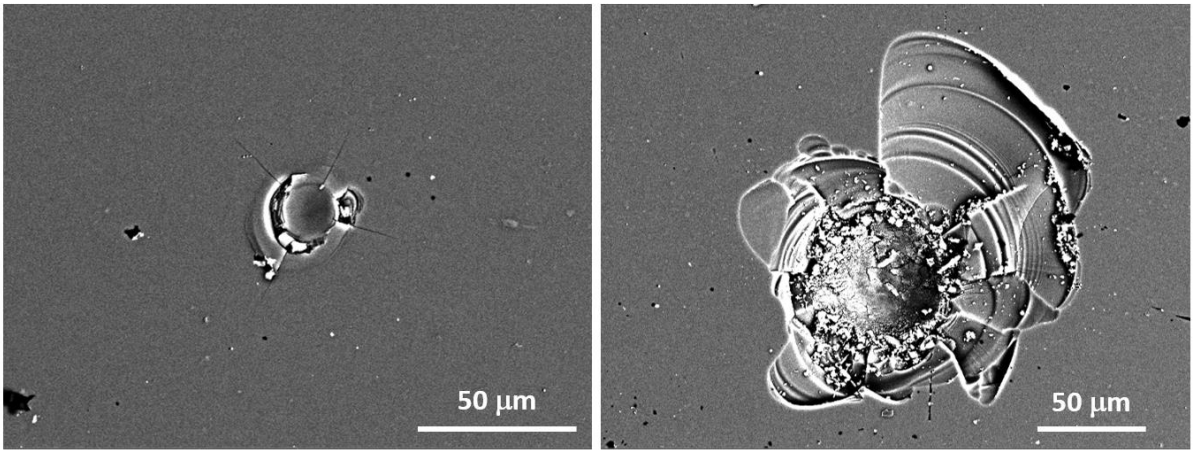
50 μm
50 μm

(c) (d)

5 (c,d)

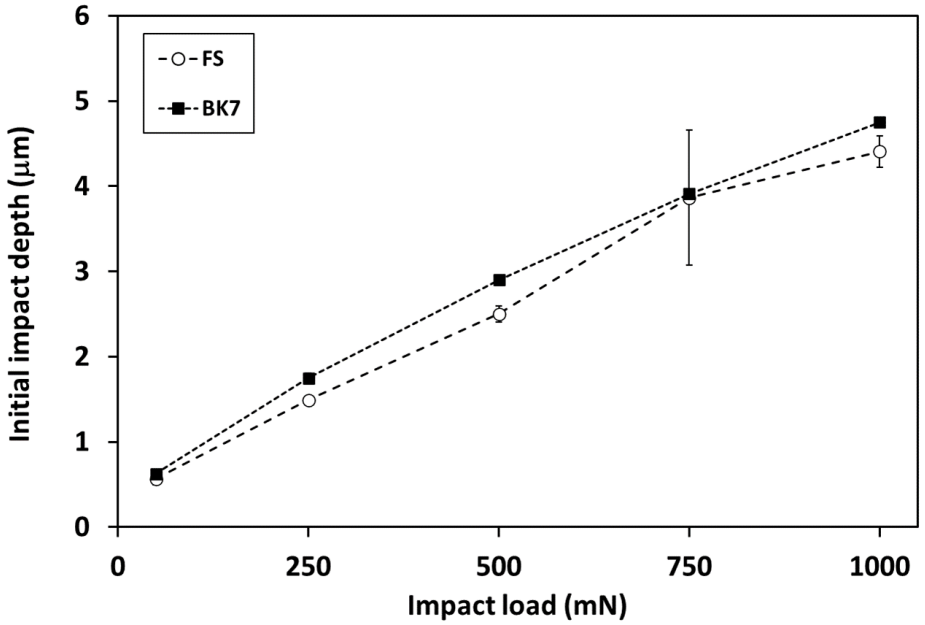
FS
BK7
Initial impact depth (μm)
Impact load (mN)
0
1
2
3
4
5
6
0
250
500
750
1000

5 (e)

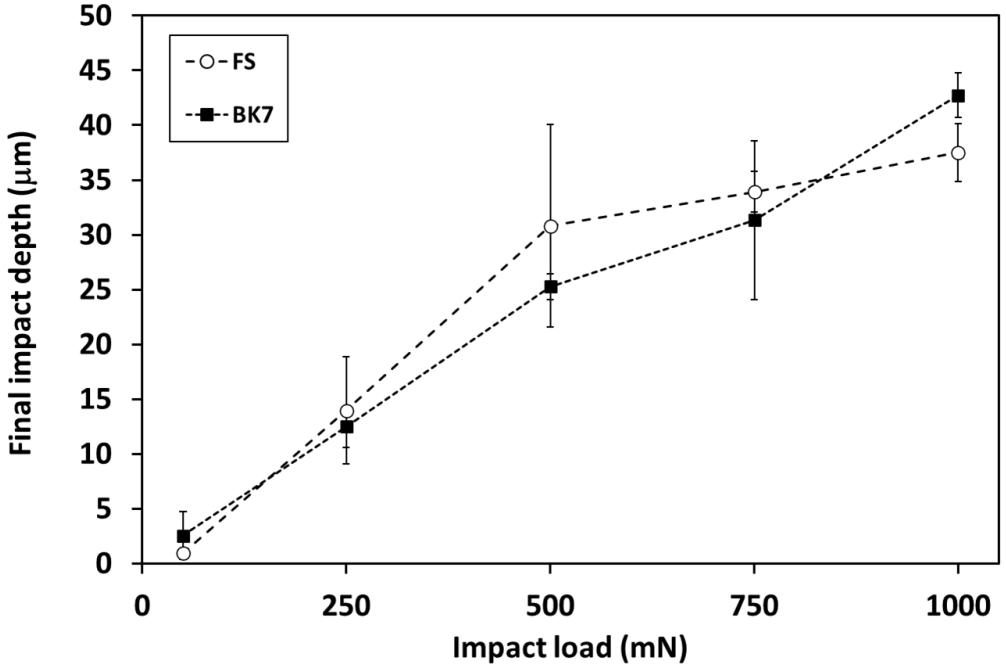
FS
BK7
Final impact depth (μm)
Impact load (mN)
0
5
10
15
20
25
30
35
40
45
50
0
250
500
750
1000

5 (f)

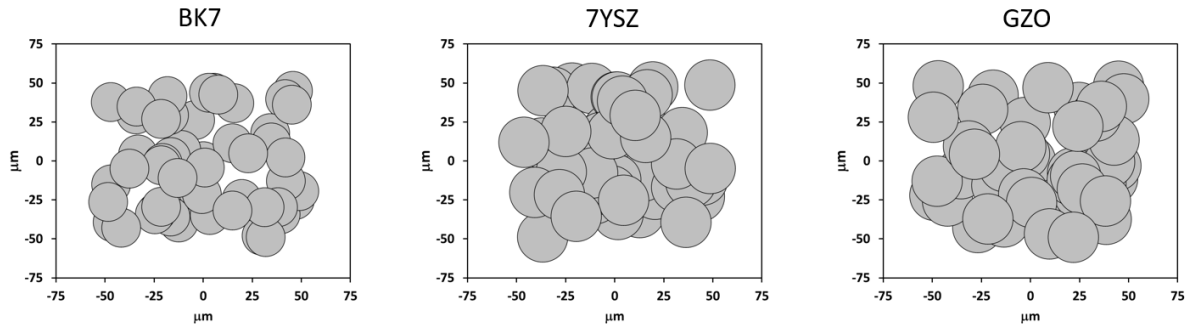
BK7
7YSZ
GZO
µm
µm
µm

6 (a)

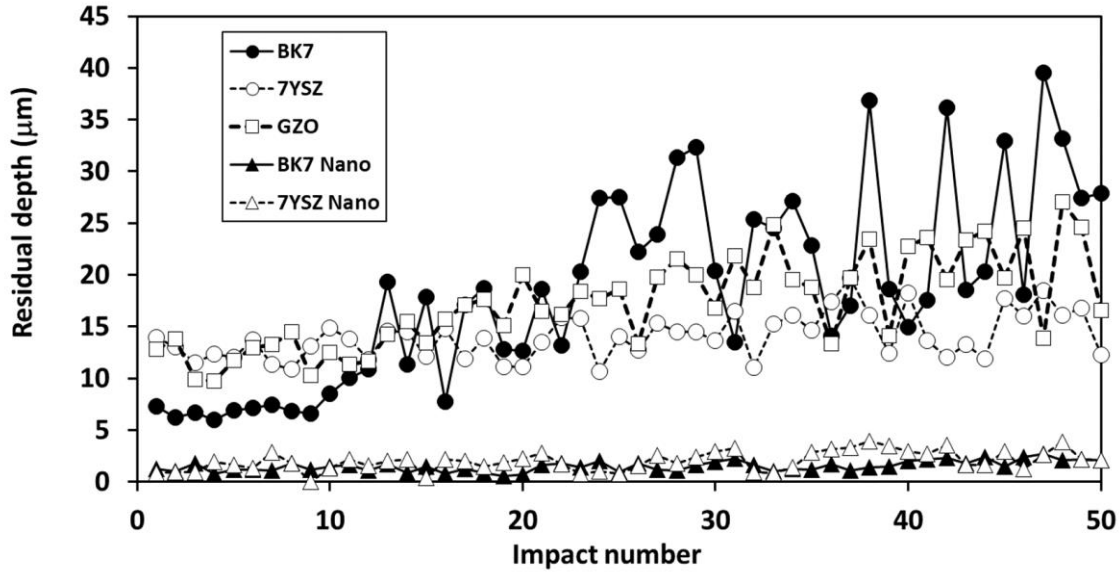
BK7
7YSZ
GZO
BK7 Nano
7YSZ Nano
Residual depth (µm)
Impact number

6 (b)

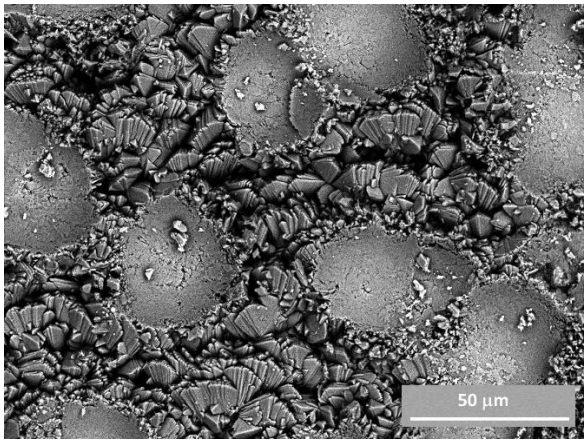
50 µm

7 (a)

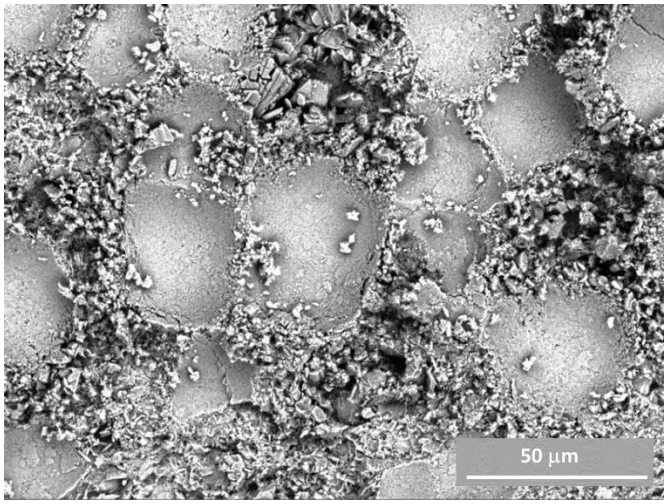

7 (b)

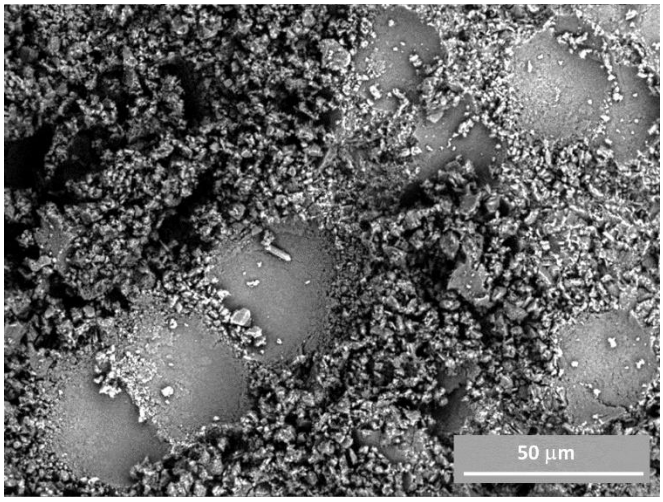

7 (c)

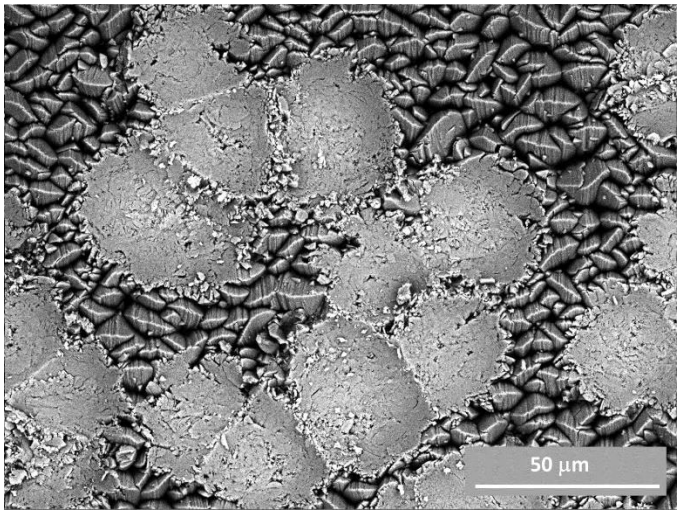

7 (d)

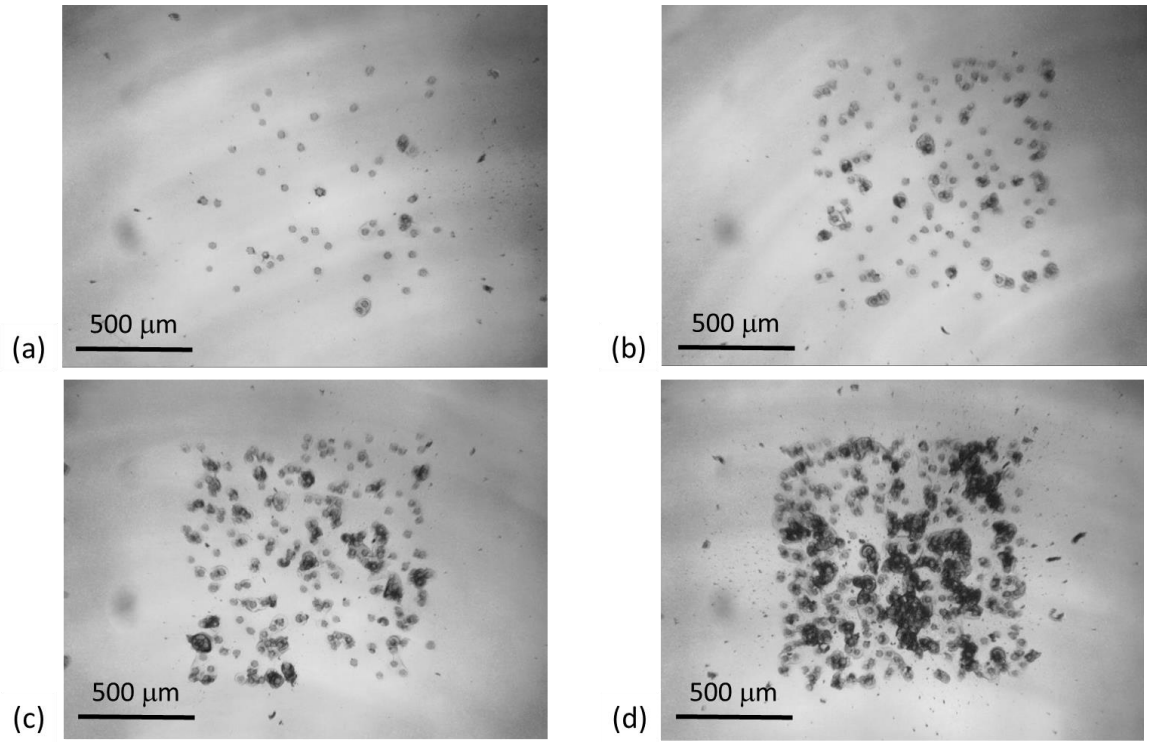

8

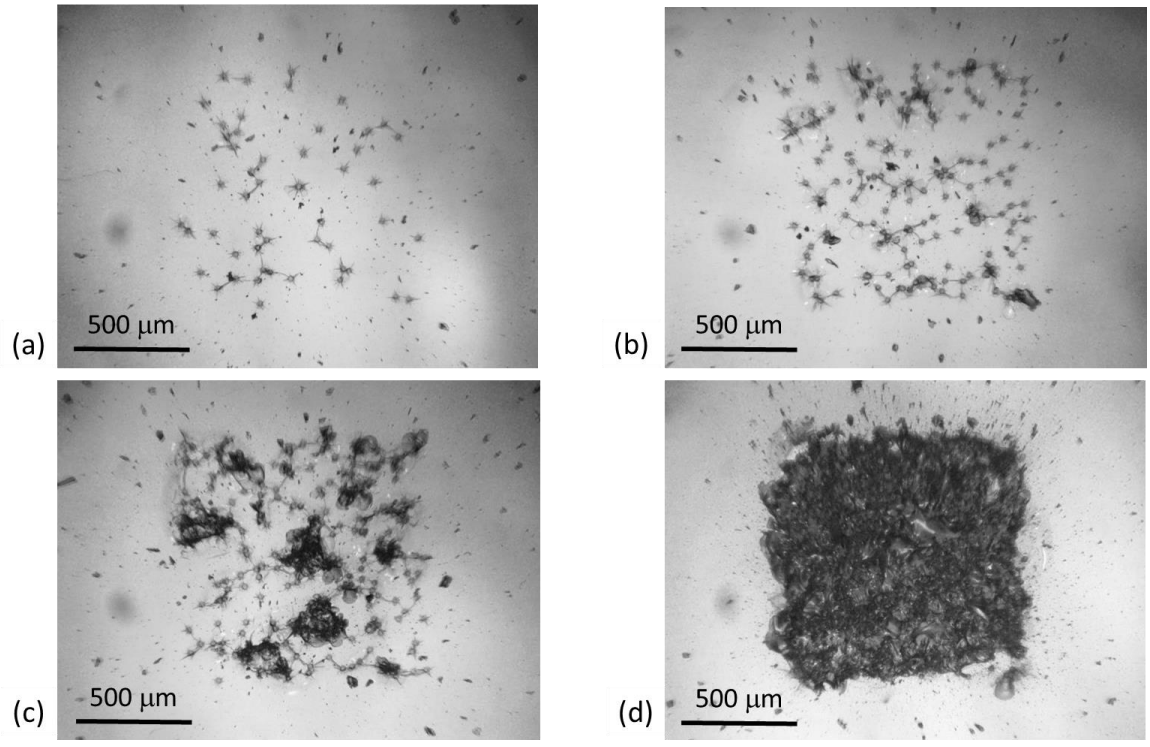

9

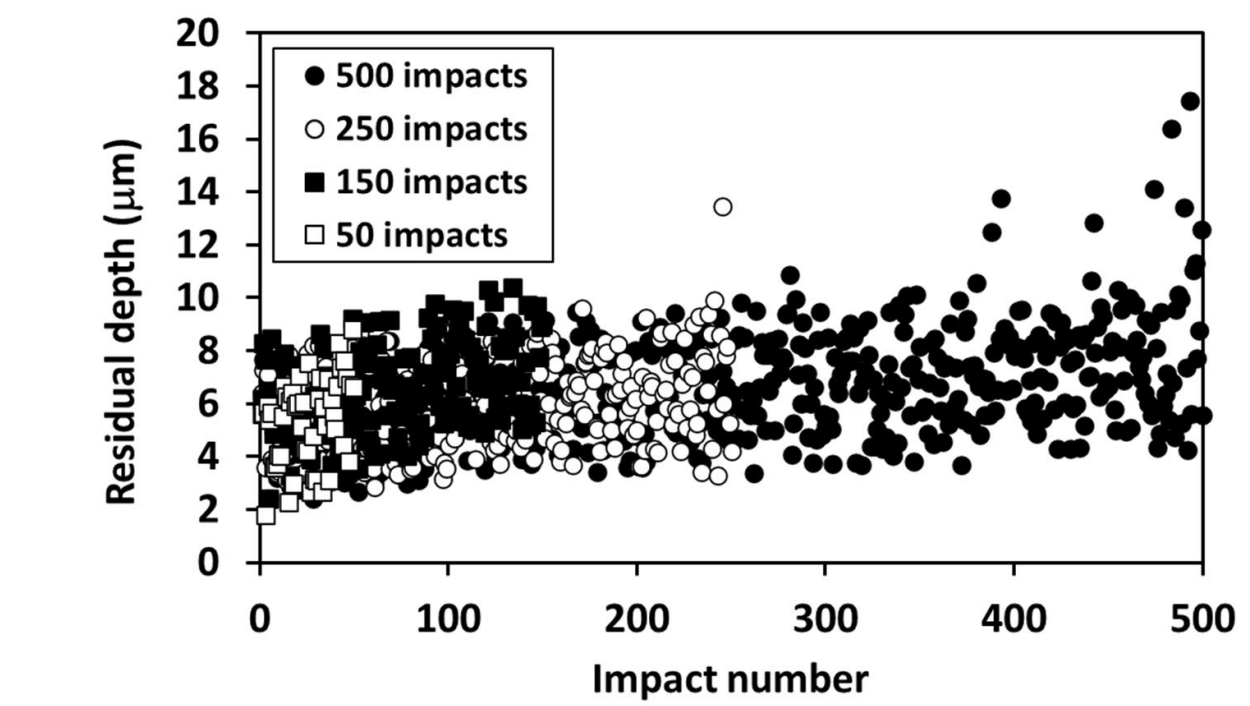
Residual depth (μm)
Impact number
500 impacts
250 impacts
150 impacts
50 impacts
0
2
4
6
8
10
12
14
16
18
20
0
100
200
300
400
500

10 (a)

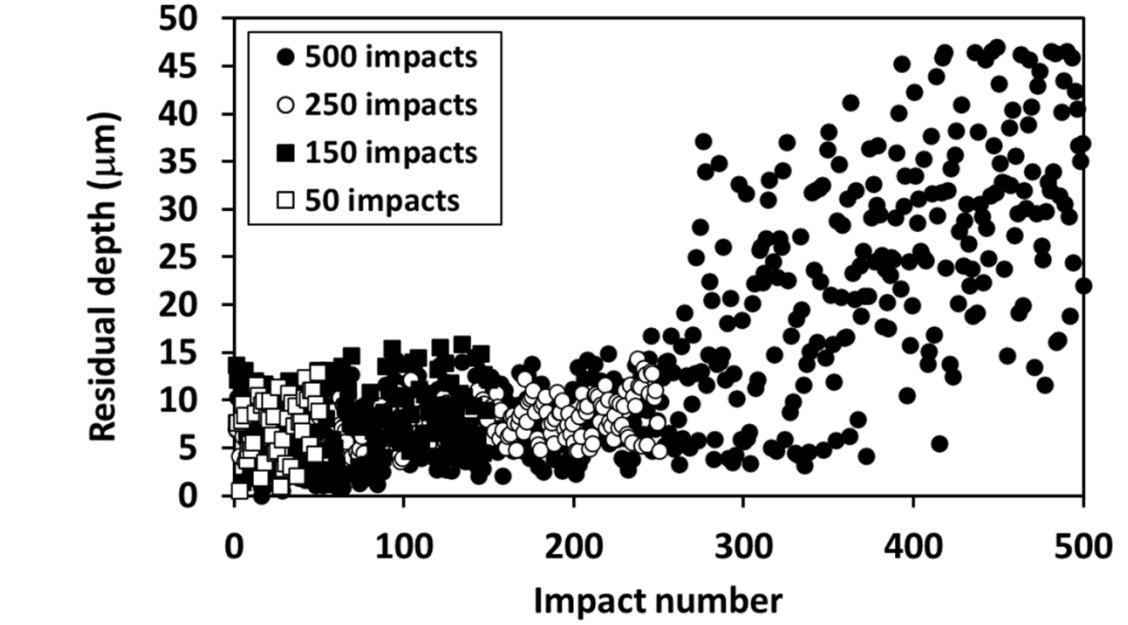
Residual depth (μm)
Impact number
500 impacts
250 impacts
150 impacts
50 impacts
0
5
10
15
20
25
30
35
40
45
50
0
100
200
300
400
500

10 (b)

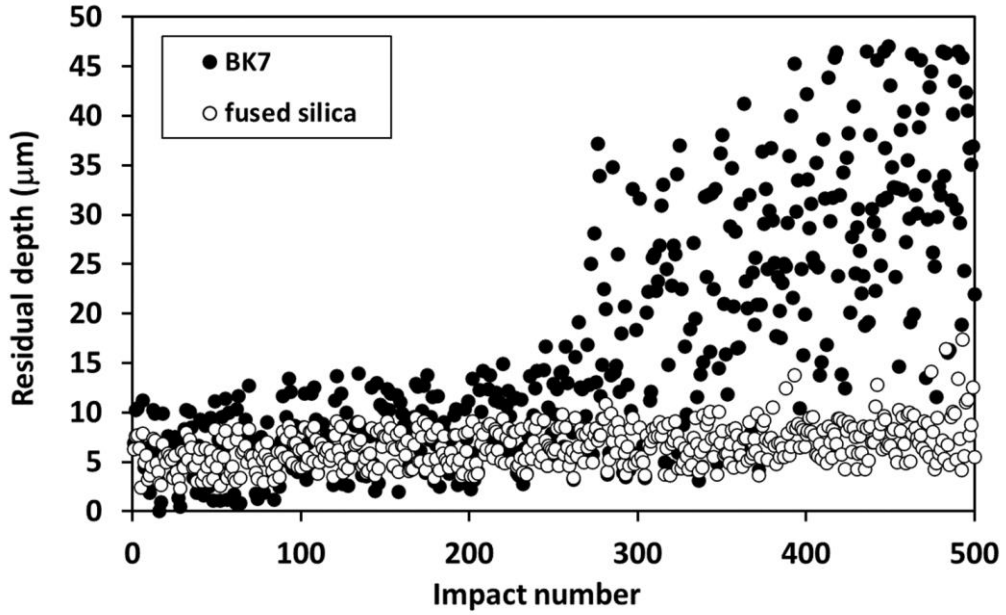
BK7
fused silica
Residual depth (μm)
Impact number
0
5
10
15
20
25
30
35
40
45
50
0
100
200
300
400
500

11 (a)

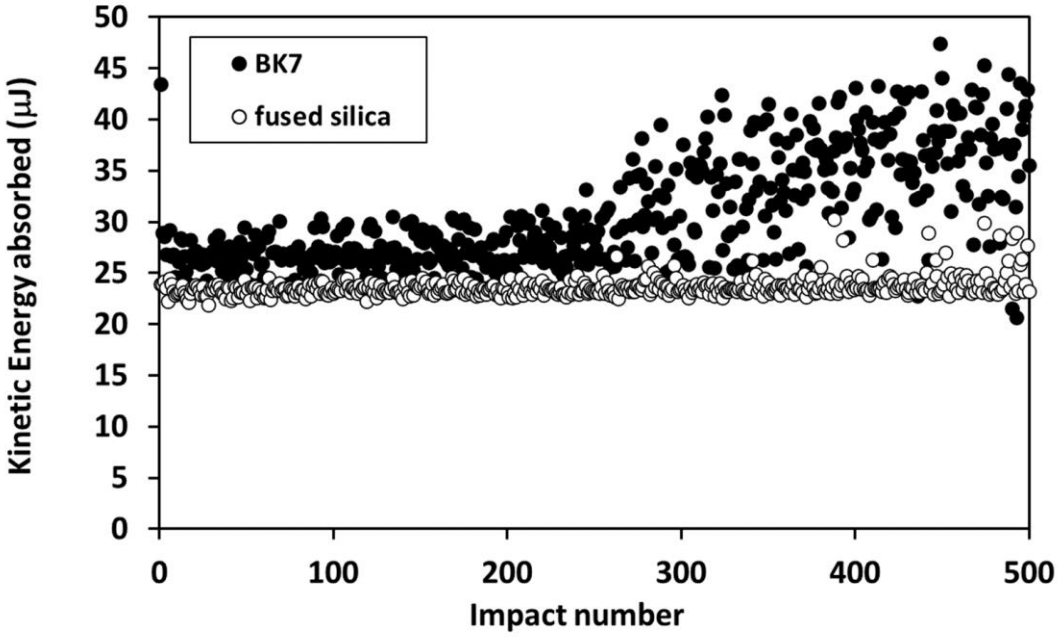
BK7
fused silica
Kinetic Energy absorbed (μJ)
Impact number
0
5
10
15
20
25
30
35
40
45
50
0
100
200
300
400
500

11 (b)

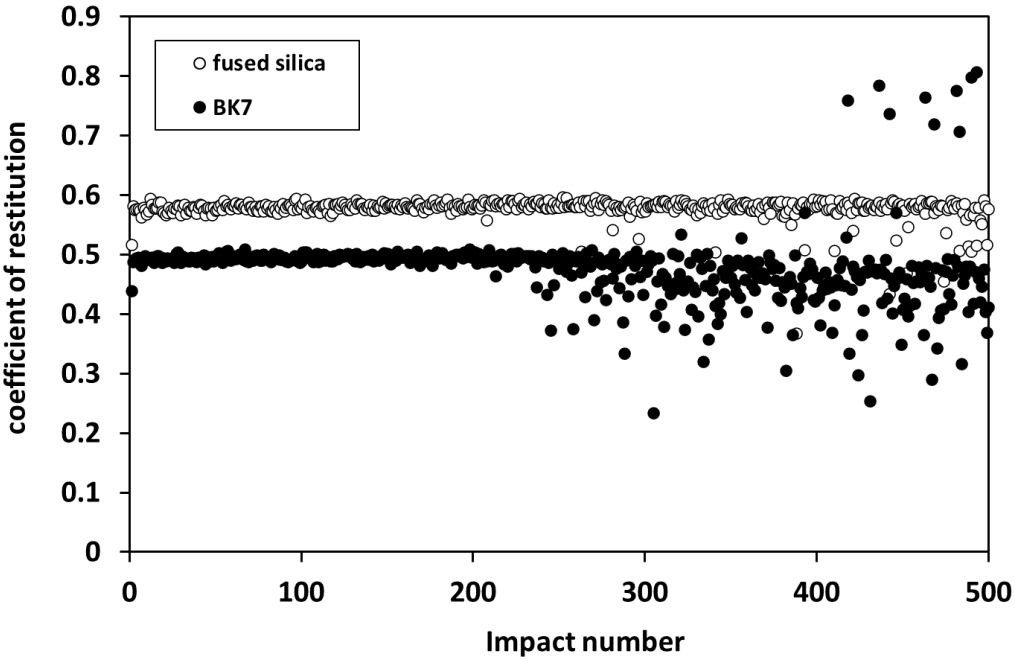
fused silica
BK7
coefficient of restitution
Impact number
0.9
0.8
0.7
0.6
0.5
0.4
0.3
0.2
0.1
0
0
100
200
300
400
500

11 (c)

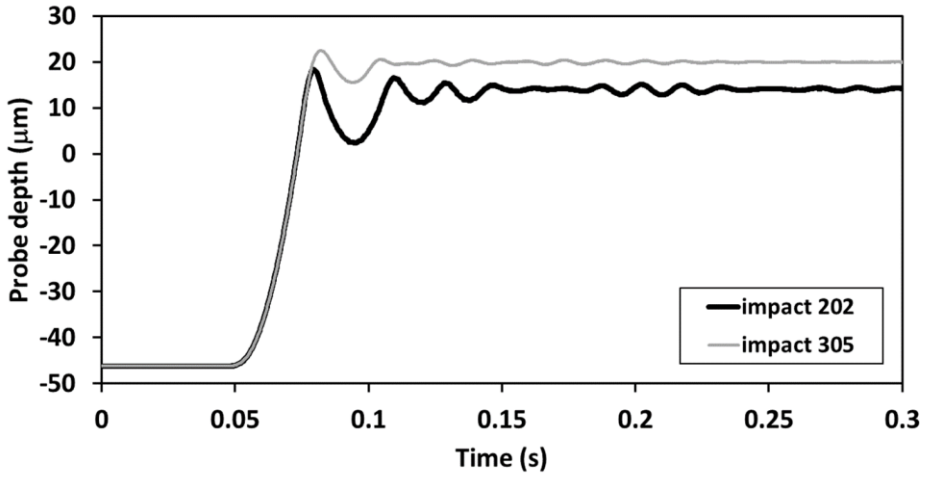
impact 202
impact 305
Probe depth (μm)
Time (s)
30
20
10
0
-10
-20
-30
-40
-50
0
0.05
0.1
0.15
0.2
0.25
0.3

12

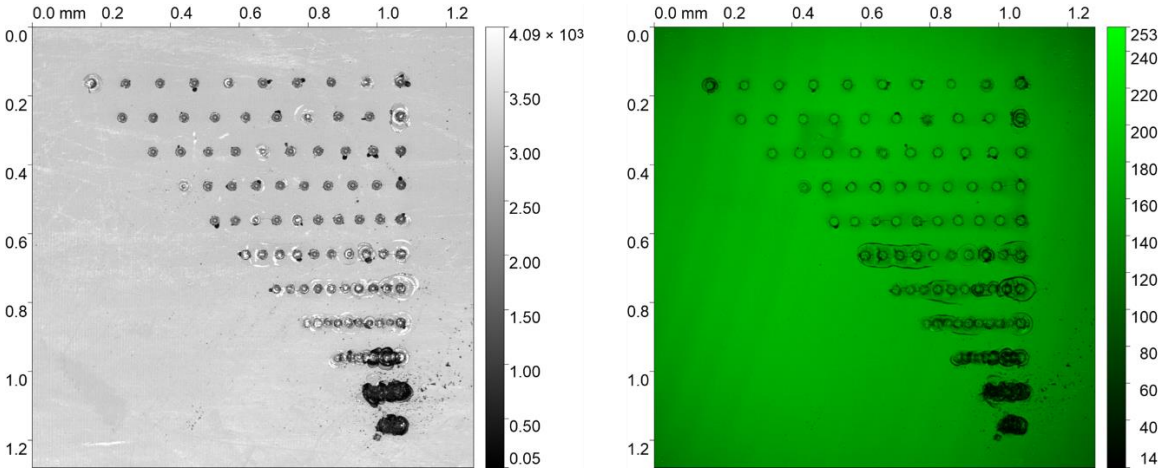

13 (a, b)

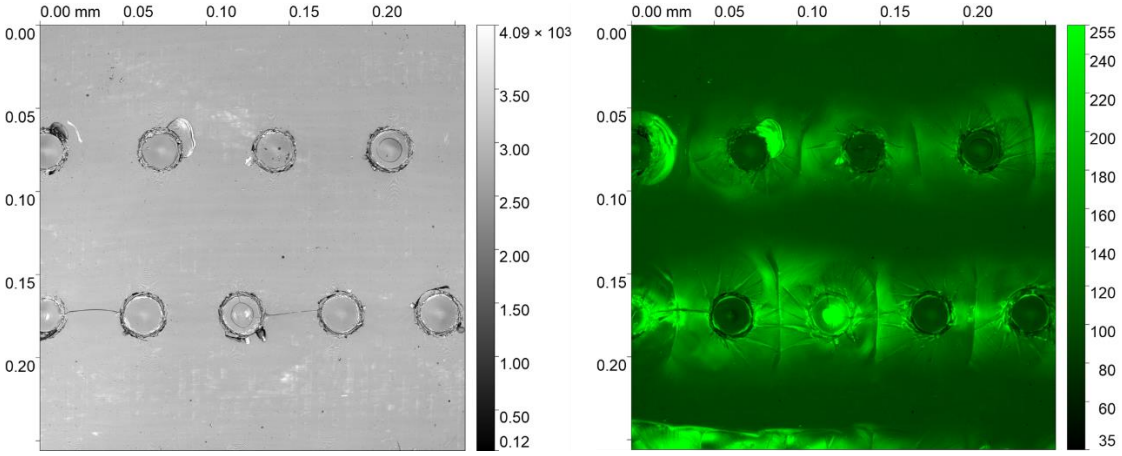

13 (c,d)

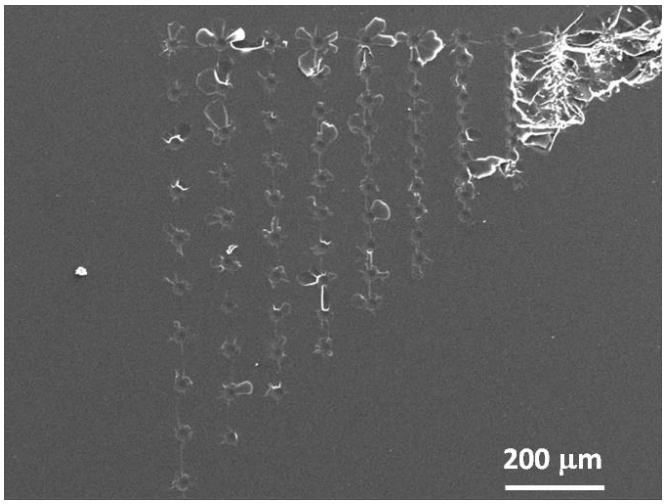

14 (a)

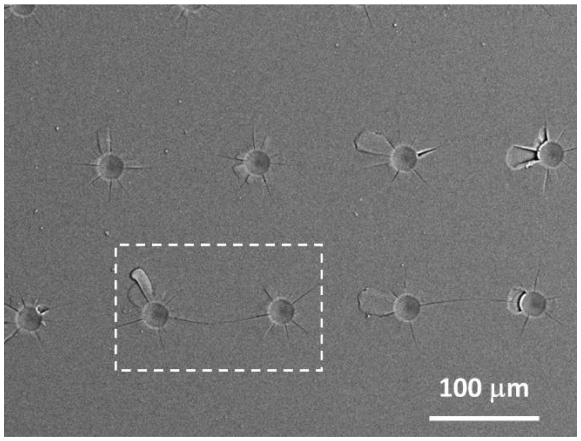
100 μm

14 (b)

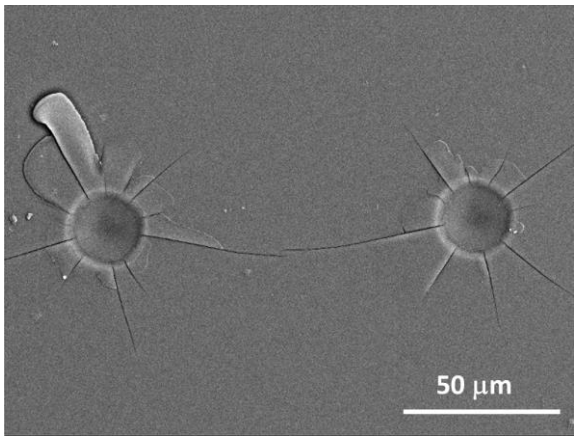
50 μm

14 (c)

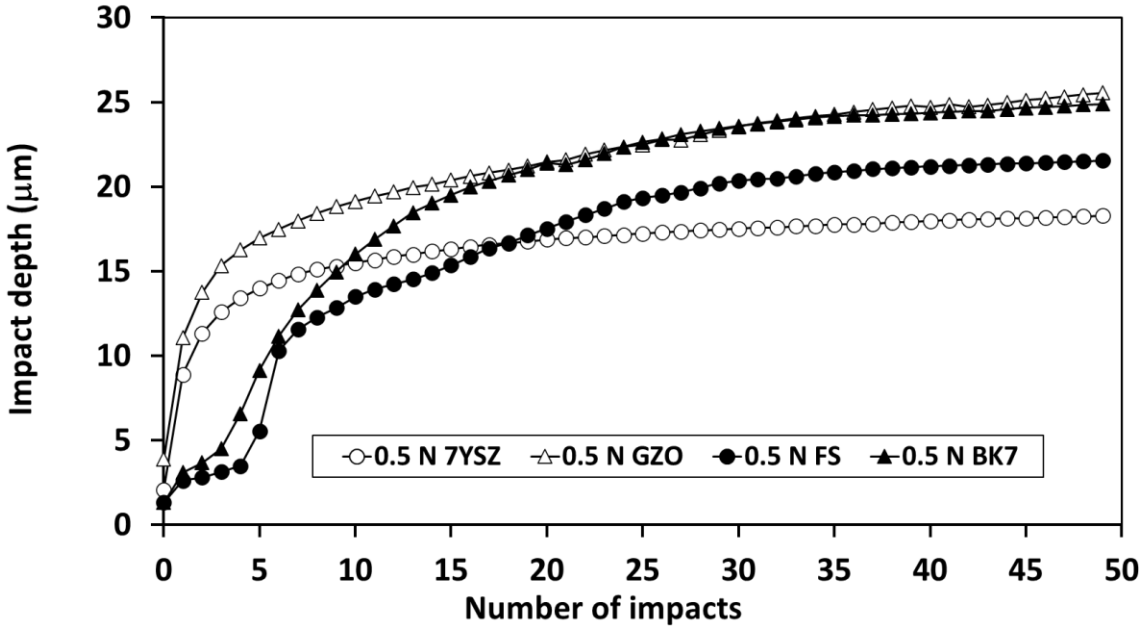
Impact depth (μm)
Number of impacts
0.5 N 7YSZ
0.5 N GZO
0.5 N FS
0.5 N BK7
0
5
10
15
20
25
30
35
40
45
50

15 (a)

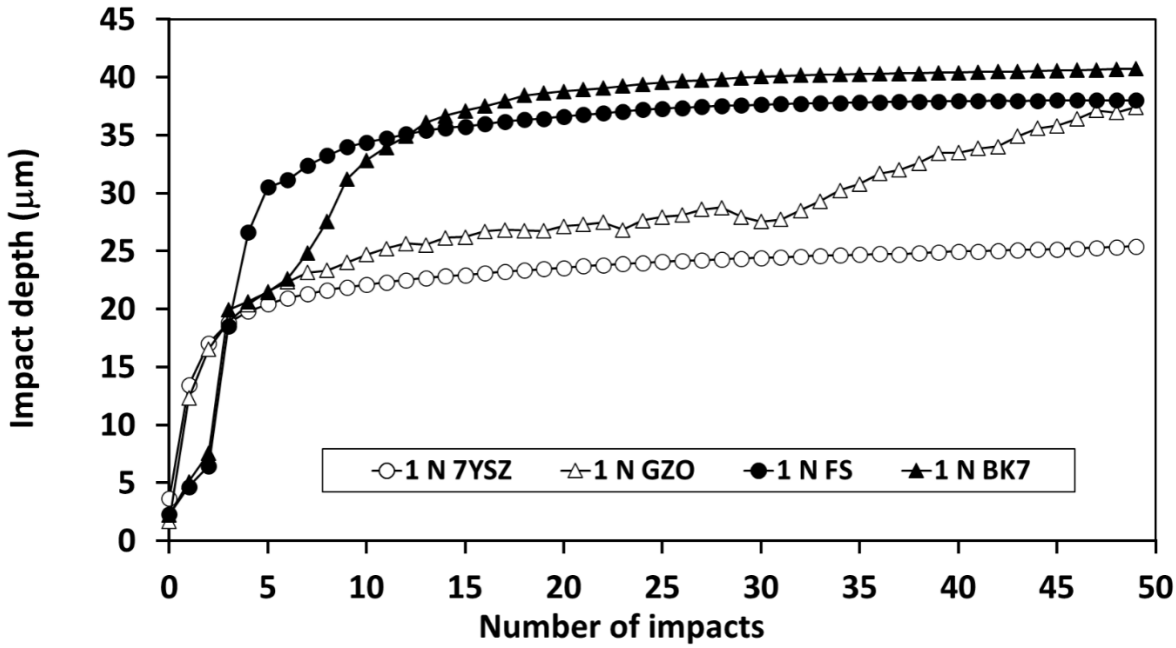

15 (b)

Randomised nano-/micro- impact testing – A novel experimental test method to simulate erosive damage caused by solid particle impacts

Beake, Ben D.

2024-07-01

Beake BD, Goodes SR, Zhang H, et al., (2024) Randomised nano-/micro-impact testing–a novel experimental test method to simulate erosive damage caused by solid particle impacts. Tribology International, Volume 195, July 2024, Article number 109647

https://doi.org/10.1016/j.triboint.2024.109647